Radiology

ORIGINAL RESEARCH • STATEMENTS AND GUIDELINES

Expanding Applications of Pulmonary MRI in the Clinical Evaluation of Lung Disorders: Fleischner Society Position Paper

Hiroto Hatabu, MD, PhD • Yoshiharu Ohno, MD, PhD** • Warren B. Gefter, MD • Grace Parraga, PhD • Bruno Madore, PhD • Kyung Soo Lee, MD, PhD • Talissa A. Altes, MD • David A. Lynch, MB, BCh • John R. Mayo, MD • Joon Beom Seo, MD, PhD • Jim M. Wild, PhD • Edwin J. R. van Beek, MD, PhD • Mark L. Schiebler, MD** • Hans-Ulrich Kauczor, MD** • For the Fleischner Society*

From the Center for Pulmonary Functional Imaging, Department of Radiology, Brigham and Women's Hospital and Harvard Medical School, 75 Francis St, Boston, MA 02115 (H.H.); Department of Radiology, Fujita Health University School of Medicine, Toyoake, Aichi, Japan (Y.O.); Department of Radiology, Penn Medicine, University of Pennsylvania, Philadelphia, Pa (W.B.G.); Department of Medical Biophysics, Western University, London, Canada (G.P.); Department of Radiology, Brigham and Women's Hospital and Harvard Medical School, Boston, Mass (B.M.); Department of Radiology, Samsung Medical Center, Sungkyunkwan University School of Medicine (SKKU-SOM), Seoul, Korea (K.S.L.); Department of Radiology, University of Missouri, Columbia, Mo (T.A.A.); Department of Radiology, National Jewish Health, Denver, Colo (D.A.L.); Department of Radiology, Vancouver General Hospital and University of British Colombia, Vancouver, Canada (J.R.M.); Department of Radiology, Research Institute of Radiology, Asan Medical Center, University of Ulsan College of Medicine, Seoul, South Korea (J.B.S.); Section of Academic Radiology, University of Sheffield, Sheffield, England, United Kingdom (J.M.W.); Edinburgh Imaging, Queen's Medical Research Institute, University of Edinburgh, Edinburgh, Scotland, United Kingdom (E.J.R.v.B.); Department of Radiology, UW Madison School of Medicine and Public Health, Madison, Wis (M.L.S.); and Diagnostic and Interventional Radiology, University Hospital Heidelberg, Translational Lung Research Center Heidelberg, member of the German Center of Lung Research, Heidelberg, Germany (H.U.K.).
Received March 27, 2020; revision requested May 20; revision received July 2; accepted July 15.
Address correspondence to H.H. (e-mail: *hhatabu@partners.org*).

*Chair and **Vice Chair of the Fleischner Society writing committee of the position paper for Pulmonary MRI.

Conflicts of interest are listed at the end of this article.

Radiology 2020; 00:1–16 • https://doi.org/10.1148/radiol.2020201138 • Content codes: CH MR

Pulmonary MRI provides structural and quantitative functional images of the lungs without ionizing radiation, but it has had limited clinical use due to low signal intensity from the lung parenchyma. The lack of radiation makes pulmonary MRI an ideal modality for pediatric examinations, pregnant women, and patients requiring serial and longitudinal follow-up. Fortunately, recent MRI techniques, including ultrashort echo time and zero echo time, are expanding clinical opportunities for pulmonary MRI. With the use of multicoil parallel acquisitions and acceleration methods, these techniques make pulmonary MRI practical for evaluating lung parenchymal and pulmonary vascular diseases. The purpose of this Fleischner Society position paper is to familiarize radiologists and other interested clinicians with these advances in pulmonary MRI and to stratify the Society recommendations for the clinical use of pulmonary MRI into three categories: *(a)* suggested for current clinical use, *(b)* promising but requiring further validation or regulatory approval, and *(c)* appropriate for research investigations. This position paper also provides recommendations for vendors and infrastructure, identifies methods for hypothesis-driven research, and suggests opportunities for prospective, randomized multicenter trials to investigate and validate lung MRI methods.

Online supplemental material is available for this article.

Pulmonary MRI has had limited clinical use for patients with lung disease, especially when compared with radiography, CT, and PET/CT. However, MRI has become practical in many countries due to advances in MRI pulse sequences, multicoil parallel imaging, and acceleration methods, along with the increased (but not universal) availability of postprocessing software. Recently, ultrashort echo time (UTE) and zero echo time proton MRI have extended the use of conventional or anatomic proton MRI for clinical examinations, and inhaled-gas methods have opened up avenues for functional lung imaging. The transition to MRI from radiography-based methods has been driven by the fact that MRI does not impart ionizing radiation, which is particularly important in younger patients with chronic illness (eg, cystic fibrosis [CF]), for young and pregnant women, or for those patients requiring extensive longitudinal follow-up (eg, severe asthma).

The purpose of this Fleischner Society position paper is to familiarize our community with recent advances in pulmonary MRI and to provide a consensus expert opinion regarding appropriate clinical indications for this modality. These opinions were initially endorsed in consensus among the writing committee members, following which the manuscript was endorsed by the Society members at large and was approved by the Fleischner Society Publication Development and Oversight Committee and the Fleischner Executive Committee before submission to *Radiology*.

Common clinical indications for pulmonary MRI were reviewed by members of the writing committee and have been divided into three groups: *(a)* group 1 indications are suggested for current clinical use of pulmonary MRI (four or more publications from multiple institutions with clinical studies of more than 100 patients); *(b)* group 2 indications are promising but require further validation or regulatory approval (two to three publications with fewer than 100 patients, those that use methods requiring further confirmation or regulatory approval, such as hyperpolarized gases); and *(c)* group 3 indications are appropriate for research investigations (clinical studies not meeting the above criteria or limited to preclinical research) (Table 1).

Background, Brief History of MRI of Lung, and Emergence of UTE and Zero Echo Time MRI Pulse Sequences

In the 1970s, Paul Lauterbur developed the first MRI scanner, for which he jointly received the 2003 Nobel Prize in Medicine or Physiology with Peter Mansfield.

Abbreviations

CF = cystic fibrosis, CI = confidence interval, COPD = chronic obstructive pulmonary disease, DW = diffusion weighted, FDG = fluorine 18 fluorodeoxyglucose, GRE = gradient echo, NSCLC = non–small cell lung cancer, SE = spin echo, UTE = ultrashort echo time

Summary

Due to technical advances in pulmonary MRI, the Fleischner Society offers its consensus recommendations for the clinical use of MRI in evaluating patients with common lung disorders.

Key Results

- Ultrashort echo time and zero echo time pulse sequences have improved pulmonary MRI, thus allowing expanded clinical applications, such as the serial imaging of children with cystic fibrosis.
- Current recommendations for the clinical use of pulmonary MRI are offered as three categories: *(a)* for current clinical use, *(b)* promising but require further validation or regulatory approval, and *(c)* appropriate for research investigations.
- Opportunities for prospective, randomized multicenter trials to investigate pulmonary MRI methods are suggested.

Much later, in 1996, Cutillo remarked that “lung imaging is a latecomer in magnetic resonance imaging” (1). The conceptual framework of the lung’s air and soft-tissue interfaces and its three-dimensional structure were investigated in the 1980s (2). The large difference in magnetic susceptibility between air and lung parenchyma results in broad frequency distributions and phase dispersion within voxels, causing an incoherent proton spectrum, noise after image reconstruction, and short T2* (3–6). Moreover, the gap in susceptibility between lung parenchyma and the chest wall manifests as a dark line perpendicular to the frequency-encoding direction. In 1991, the phenomenon of susceptibility effects was described in detail, and potential solutions were proposed using projection reconstruction MRI with UTE (7–9). But this solution required more than 2 decades of hardware and software improvements before successful clinical implementation was possible (10–12). Clinical MRI of the lung has since been pursued using spin-echo (SE) and gradient-echo (GRE) sequences with short echo time and half-Fourier single-shot fast SE sequences (13–15). MRI of the pulmonary vasculature is possible using electrocardiographic gating, surface coils, and cine GRE MRI (16,17).

In 1994, ventilation MRI using hyperpolarized xenon 129 (^{129}Xe) was first reported in small animals (18). In 1996, hyperpolarized helium 3 (^{3}He) MRI was pioneered in healthy volunteers and participants with lung disease (19,20), and contrast material–enhanced perfusion MRI emerged (21). This was followed by reports using perfusion parametric mapping with three-dimensional imaging and breath holding (22–24). Dynamic oxygen-enhanced proton ventilation MRI was also introduced and shown to be highly correlated with measurements of the diffusing capacity of the lung for carbon monoxide (25–27). In 2009, unenhanced perfusion and ventilation proton MRI using Fourier decomposition were pioneered (28).

Despite these advancements in the field of pulmonary functional imaging, there has been limited clinical utilization of pulmonary MRI, primarily due to the benefits provided by high-resolution CT, which include speed, availability, familiarity, ease of access, and superb natural contrast and spatial resolution of the lung parenchyma. In contradistinction to CT, pulmonary MRI has a longer acquisition time with sensitivity to respiratory motion and is affected by the lung’s lower proton density and aforementioned susceptibility effects from air and soft-tissue interfaces.

Nevertheless, pulmonary MRI is poised to become a primary clinical imaging modality due to the development of UTE and zero echo time sequences, which have been “game changers” for pulmonary MRI. These sequences provide a higher signal-to-noise ratio from the lung’s relatively short T2*. Their evolution, from longer to shorter echo times, is described in Figure 1 and explained in detail in Appendix E1 (online).

Clinical Indications for Pulmonary MRI

Data Support Current Clinical Application (Suggested for Current Clinical Use)

Evaluation of CF.—CF manifests with pulmonary pathologic findings from birth. Pulmonary MRI can demonstrate the presence of bronchiectasis and mucus plugging in CF, but imaging is challenging because of the great range in patient age as well as disease severity in this population, due to the different classes of CF transmembrane conductance regulator mutations and exogenous factors such as bacterial colonization. These variations in CF result in different degrees of disease severity, but therapeutic agents, including modulators and potentiators, may extend life expectancy for individuals with CF.

To our knowledge, only in Germany has proton MRI been introduced into the routine clinical management and long-term monitoring of patients with CF as the standard of care. Similar to CT, proton MRI provides morphologic information with respect to mucus distribution, bronchiectasis, inflammatory airway wall thickening, consolidation, and atelectasis, and it depicts disease activity from birth (29–31) (Fig 2). Inspiratory and expiratory three-dimensional GRE MRI reveals air trapping (32) as a low spatial resolution radiation-free alternative to inspiratory and expiratory CT, although steady-state free precession methods can be used to distinguish mucus from airway wall thickening (33). An MRI scoring system, similar to CT scoring systems, may help grade disease severity (34). MRI can also reveal perfusion abnormalities caused by hypoxic pulmonary vasoconstriction with high sensitivity that reflects ventilation impairment due to airway obstruction (Euler-Liljestrand reflex) (35). MRI perfusion defects can reveal even a small airway (<1 mm in diameter) obstruction, which is difficult if not impossible to detect using CT. For example, CT demonstrated only 20% of potentially detectable perfusion abnormalities in young patients with CF (30). In addition, MRI perfusion defects correlated with the multiple breath wash-out lung clearance index measurement in young children and adolescents (36). Also, two single-center studies showed that mucus plugging, consolidation, and perfusion abnormalities were increased in pulmonary exacerbations of CF and reversed after antibiotic therapy (30,36,37). A multicenter MRI study in young children with CF also showed that lung clearance index values

Table 1: Summary of Clinical Indications for Pulmonary MRI

Data Support Current Clinical Application	Data Promising: Further Validation or Regulatory Approval Required	Investigational
Cystic fibrosis	Pulmonary embolism	Chronic obstructive pulmonary disease
Lung cancer staging	Pulmonary parenchymal abnormalities	
Lung nodule characterization		Asthma
Pulmonary hypertension	Lung nodule detection	Interstitial lung disease

had a moderate to strong correlation with the MRI scores (38).

Hyperpolarized gas MRI with ^{3}He reveals ventilation abnormalities with a high sensitivity in patients with CF (39,40) who have normal spirometry and normal CT (41). Quantification of ventilation defects is feasible and may be useful for monitoring therapy effectiveness (42). This, in combination with the fact that hyperpolarized ^{3}He is more sensitive to lung function decline than pulmonary function tests(43), highlights its value in helping detect very early lung disease. Preliminary therapy studies using hyperpolarized ^{3}He ventilation as an end point showed response to a CF transmembrane conductance regulator gene potentiator in parallel with changes in forced expiratory volume in 1 second (39), but very few studies support MRI use in very young children, to our knowledge (44). MRI with hyperpolarized ^{129}Xe is less costly than hyperpolarized ^{3}He and shows promise for clinical use in specialist CF centers (37,45–48), including evaluation of treatment responses and correlation with pulmonary function measurements such as lung clearance index. Unenhanced MRI methods for perfusion and/or ventilation imaging (eg, arterial spin labeling, echo time–dependent mapping of T1 relaxation times, and Fourier decomposition MRI) also provide alternatives for CF lung ventilation and perfusion measurements (49–51). The next area of research will need to focus on how MRI results change patient outcomes (eg, life expectancy, hospitalization length of stay, cost of care) compared with CT and its cost effectiveness.

In conclusion, proton-based pulmonary MRI for longitudinal assessment of patients with CF is the current clinical standard in Germany, and data support its more widespread use in patients with CF. The use of hyperpolarized gas remains an important research tool, awaiting regulatory approval for clinical use beyond the United Kingdom.

Lung cancer and lung nodule characterization.—Early lung cancer detection and pulmonary nodule characterization are important challenges for radiology. Although CT serves as the clinical workhorse, MRI plays a role in specific clinical scenarios. Various MRI techniques, such as SE sequences, including short inversion time inversion recovery, turbo SE sequence, and GRE sequences, yield detection rates ranging from 26% to 96% (52–55). Recently, three-dimensional GRE sequences with UTE (echo time, less than 200 μsec) enabled a detection rate of greater than 90% for nonsolid, part-solid, and solid nodules ranging from 4 to 29 mm in diameter, thus challenging thin-section CT in nodule detection (54). In a recent study, the potential of MRI as a screening tool for lung cancer was compared with low-dose CT (56) for 224 lung cancer screening participants with nodules of 4 mm or greater; patients were then assigned a Lung Imaging Reporting and Data System category. All eight cancers were accurately depicted with MRI. The Lung Imaging Reporting and Data System score was overestimated with MRI in one patient for category 4A, two patients for category 3, and five patients for category 2 nodules. The authors concluded that MRI was comparable to low-dose CT in a lung cancer screening program (56). The use of UTE pulse sequences has improved the detection of small lung nodules at MRI (57). This free-breathing method allows for the better delineation of lung parenchymal structure than routine breath-hold GRE techniques (57).

After detection, characterizing the potential for malignancy is pivotal. Numerous MRI sequences have been evaluated for pulmonary nodule characterization (58). Currently, diffusion-weighted (DW) MRI is considered the most useful, with a meta-analysis pooled sensitivity and specificity of 83% and 80%, respectively, in the differentiation between malignant and benign lesions (59). Some studies have shown that dynamic contrast-enhanced MRI has greater specificity and accuracy than PET/CT (60,61) (Fig 3). When DW MRI and fluorine 18 fluorodeoxyglucose (FDG) PET/CT were compared in a meta-analysis for diagnosis of the same nodule, DW MRI yielded an area under the receiver operating characteristic curve of 0.93 (95% confidence interval [CI]: 0.90, 0.95) versus 0.86 (95% CI: 0.83, 0.89) for FDG PET/CT (P = .001). This meta-analysis also showed a diagnostic odds ratio of 50 (95% CI: 19, 132) for DW MRI, which was superior to that of PET/CT (odds ratio = 15; 95% CI: 7, 32; P = .006) (62). Thus, current data show that DW MRI outperforms FDG PET/CT in the characterization of solitary pulmonary nodules.

Currently, CT and FDG PET/CT are used for lung cancer staging (tumor, node, metastasis or TNM system), and MRI is rarely employed, and typically only for selected problem solving. Although MRI had originally been proposed as superior to CT for T factor evaluations (63–66), short inversion time inversion-recovery turbo SE MRI and/or DW MRI are as helpful as PET/CT for N factor evaluation in non–small cell lung cancer (NSCLC) (67–79). Short inversion time inversion-recovery turbo SE MRI is also more sensitive and accurate than DW MRI and PET/CT (75). When both MRI and PET/CT data are available, inclusive criteria (positive for nodal metastasis either at MRI or at PET/CT) improve the sensitivity for detecting nodal metastasis compared with PET/CT alone, and they may decrease unnecessary open thoracotomy, mediastinoscopy, or endobronchial US (80). Another meta-analysis identified better diagnostic performance for MRI compared with FDG PET/CT

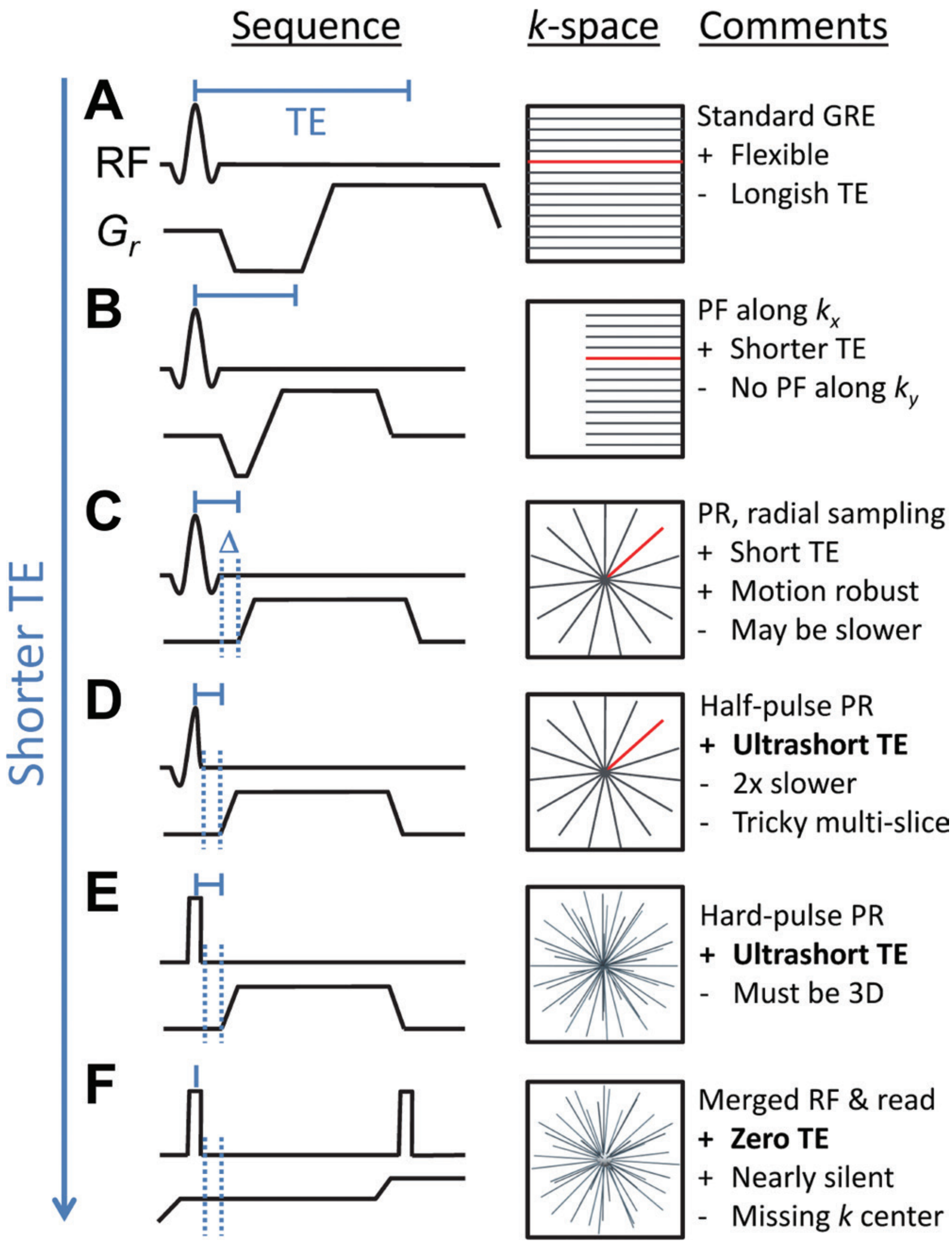

Figure 1: Diagram illustrates the race toward shorter echo time (TE) values. The evolution of echo times has involved regular MRI pulse sequences with, *A–C*, short TE setting, followed by, *D, E*, specially designed ultrashort echo time and, *F*, zero echo time sequences. Echo time is defined as time between excitation of magnetization and sampling of central k-space region. With typical MRI hardware, a minimum amount of time is required to switch between radiofrequency (RF) transmission (radiofrequency pulses) and radiofrequency reception (readout window), called Δ here and depicted greatly exaggerated in *C–F*. Δ can be a limiting factor in how small echo times can get, and a Δ of 5 μsec might be considered typical. Due to finite width of radiofrequency pulse and of Δ, a central region in k-space cannot be sampled by zero echo time pulse sequences; this is depicted in *F* using a small silvery sphere at origin of radial pattern. GRE = gradient echo, PF = partial Fourier, PR = projection reconstruction, 3D = three-dimensional.

on a per-node and per-patient basis (79). Thus, the current evidence supports the broader clinical use of MRI for TNM staging in patients with NSCLC (Fig 4). Tables 2 and 3 show reported diagnostic performances of dedicated MRI for T and N factor assessments in patients with NSCLC.

Whole-body MRI also provides acceptable accuracy and efficacy for NSCLC staging compared with whole-body PET/CT. Although whole-body MRI is more useful for depicting brain and hepatic metastases, PET/CT is more useful for the detection of lymph node and soft-tissue metastases (81). Currently, lung cancer staging may use both brain MRI and whole-body PET/CT. With available whole-body MRI data, the coregistered PET/MRI may serve as a staging tool. NSCLC was correctly upstaged in 37 of 143 patients (26%) in the PET/MRI group compared with 26 of 120 patients (22%) in the PET/CT plus brain MRI group (95% CI: –6%, 15%; P = .43), which was an insignificant difference (82). Integrated (simultaneous, rather than registered) PET/MRI can also be used as a possible adjunct to FDG PET/CT for clinical NSCLC staging with comparable staging performance (83,84).

In conclusion, studies support the utility of MRI for the characterization of known lung nodules and lung cancer staging as potential alternatives to PET/CT. Although UTE results are promising for lung nodule detection, confirmatory studies are required.

Pulmonary hypertension.—The European Society of Cardiology and European Respiratory Society issued a recent consensus statement on the diagnosis and treatment of pulmonary hypertension (85,86). Dynamic contrast-enhanced lung perfusion MRI has similar sensitivity and specificity to both planar scintigraphy (87) and SPECT (88) in its ability to screen for chronic thromboembolic pulmonary hypertension. The right ventricle is not well designed for acute pressure overload and decompensates into cor pulmonale after exposure to chronic pressure (and/or volume) overload (89). The findings of septal flattening, delayed contrast enhancement of the septal insertions, and an elevation in the right ventricular end diastolic volume index have prognostic value in pulmonary hypertension (90–93). Quantitative contrast-enhanced MR angiography is useful for the assessment of the severity of pulmonary hypertension and the longitudinal assessment of therapy ef-

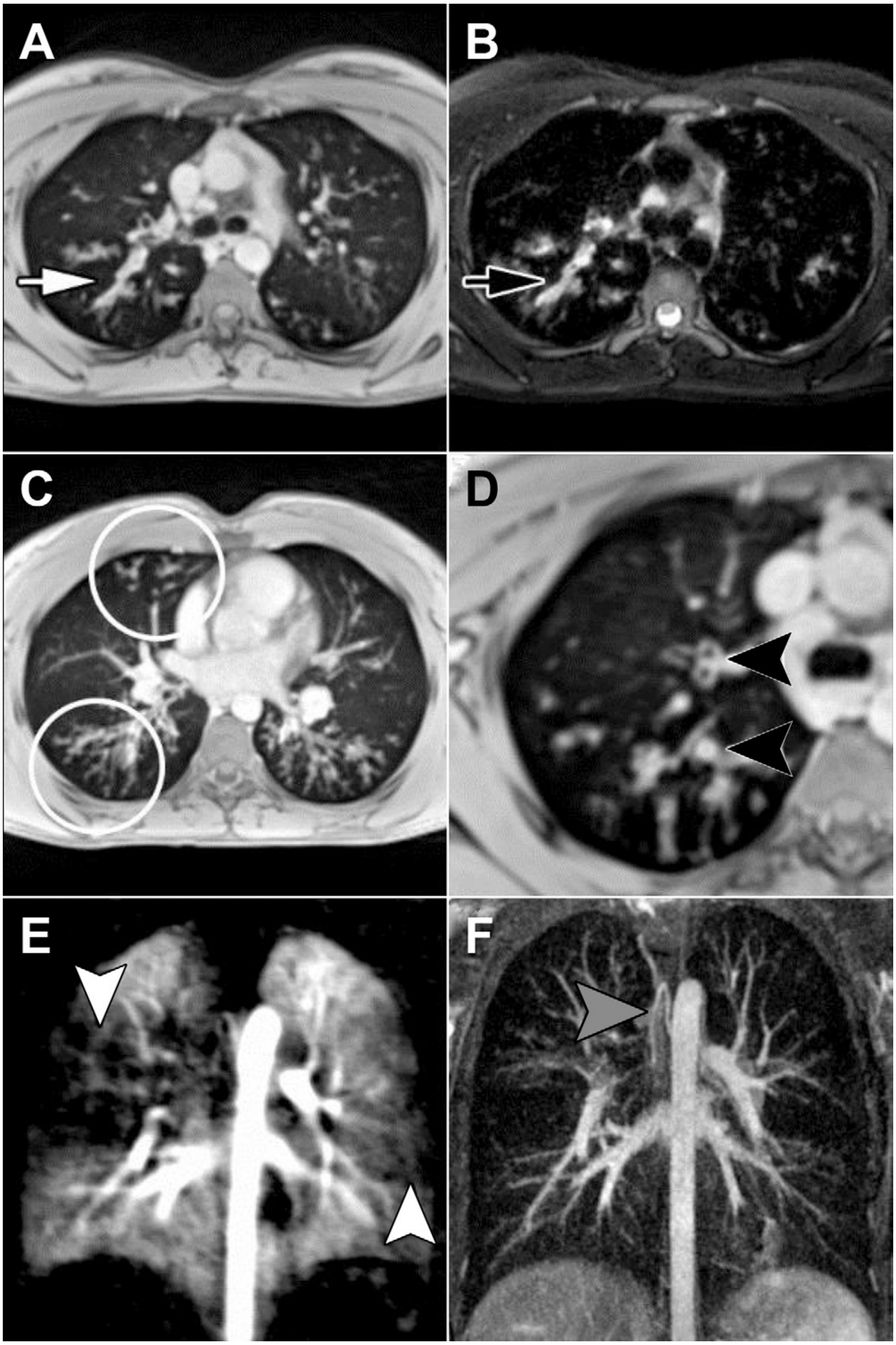

Figure 2: Typical constellation of imaging findings in an adolescent female patient with cystic fibrosis. *A*, Contrast-enhanced T1-weighted image shows mucus-filled bronchoceles (arrow) dominant in upper lobes and superior segments of lower lobes. *B*, Fat-saturated T2-weighted image best depicts mucus plugging (arrow). *C*, Maximum intensity projection of contrast-enhanced T1-weighted imaging shows tree-in-bud pattern of small airways disease (circles). *D*, Contrast-enhanced T1-weighted imaging may help differentiate airway wall inflammation (anterior black arrowhead) from mucus (posterior black arrowhead) by different signal intensities. *E*, Subtraction map from dynamic contrast-enhanced MR perfusion reveals perfusion abnormalities (arrowheads). *F*, Contrast-enhanced MR angiography shows dilated bronchial arteries (arrowhead).

fect (24,94–96) (Fig 5) (Table E1 [online]). Contrast-enhanced MR angiography has been used in the setting of chronic thromboembolic pulmonary hypertension for the diagnosis of proximal arterial enlargement, webs of chronic thrombi, and amputation of the smaller pulmonary arterial branches. Bright-blood, steady-state free precession imaging can also be used to delineate thrombus in the major pulmonary vessels in patients with chronic thromboembolic pulmonary hypertension (97) and to reveal decreased flow in the pulmonary artery due to pulmonary hypertension (98). The distensibility (relative area change) in the pulmonary artery is predictive of outcomes in patients with pulmonary hypertension (97,99), while the right ventricular end diastolic volume index and pulmonary artery area predict survival (100), as confirmed with meta-analysis (101).

In conclusion, strong evidence supports the current clinical use of cardiopulmonary MRI in patients with pulmonary hypertension.

Data Promising but Requiring Further Validation or Regulatory Approval

Pulmonary embolism.—Since 2004, pulmonary contrast-enhanced MR angiography has revealed both the direct signs of pulmonary embolism within pulmonary arteries and lung perfusion using parallel imaging techniques, time-resolved, or four-dimensional contrast-enhanced MR angiography (Fig E2 [online]) (102,103). This technique can be considered as an alternative to CT angiography for patients presenting with signs and symptoms of pulmonary embolism. In the clinical setting of suspected pulmonary embolism, single-center results for the primary use of MR angiography for the diagnosis of pulmonary embolism in 675 patients at low to intermediate risk showed patient outcomes using MR angiography as the primary diagnostic test were similar to CT angiography at 6 months of follow-up (104). Important technical developments since the Prospective Investigation of Pulmonary Embolism Diagnosis III

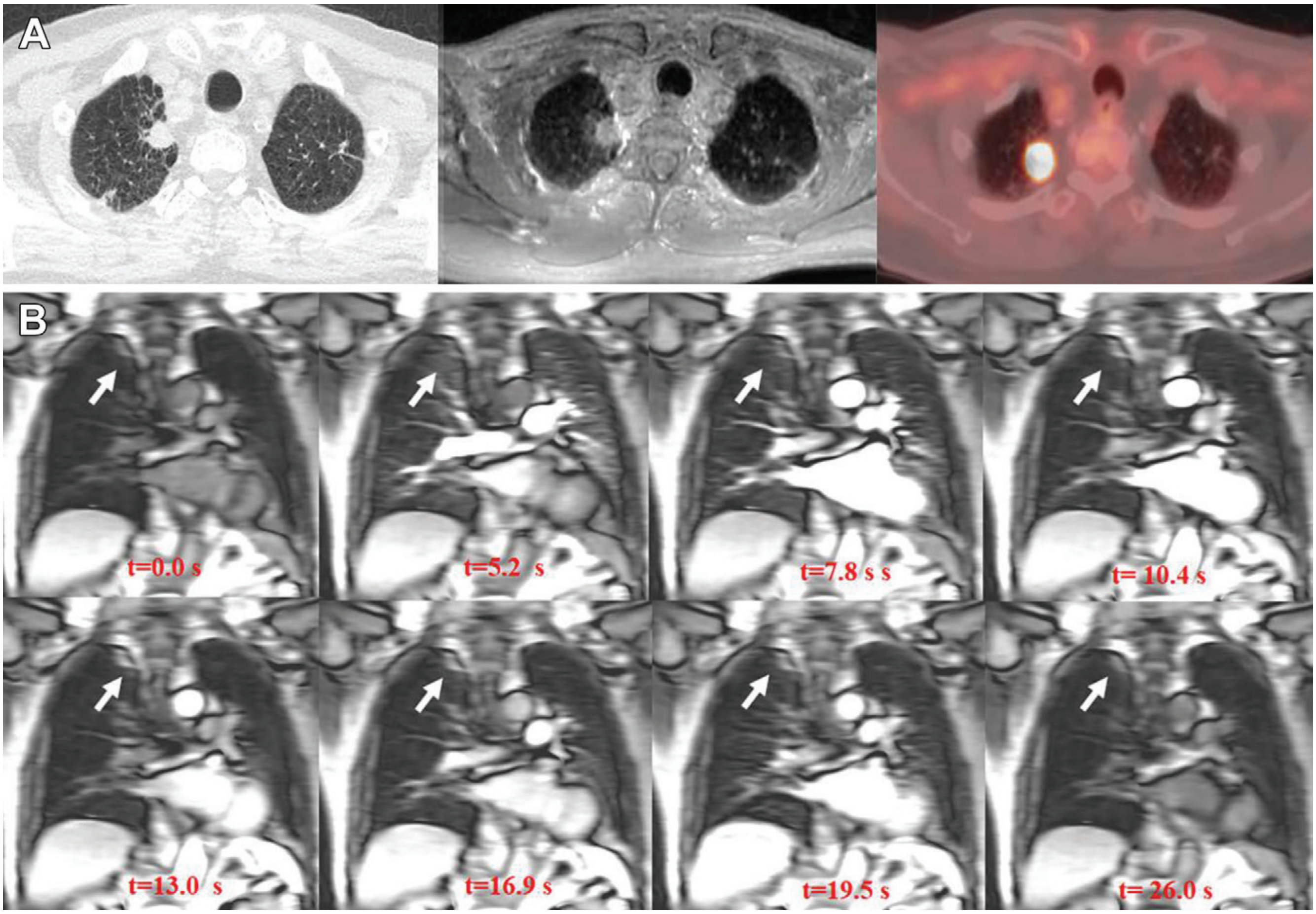

Figure 3: Images in 82-year-old man with invasive adenocarcinoma in right upper lobe. *A*, Thin-section CT scan with 1-mm-thick sections (left), pulmonary MRI scan with ultrashort echo time at 110 μsec and 1-mm-thick sections (middle), and fluorine 18 fluorodeoxyglucose (FDG) PET/CT scan with 2.5-mm-thick sections (right). CT and MRI scans show solid nodule with notch. This nodule demonstrates high FDG uptake on PET/CT scan. CT and MRI scans also show bullae and emphysematous lung surrounding tumor. *B*, Dynamic first-pass contrast material–enhanced perfusion gradient-echo MRI scans obtained with a 3-T system demonstrate well-enhanced nodule (arrows) in right upper lobe. This nodule shows enhancement from lung parenchymal phase and is well enhanced at systemic circulation phase. *t* is the time after injection of gadolinium-based contrast agent followed by saline chaser.

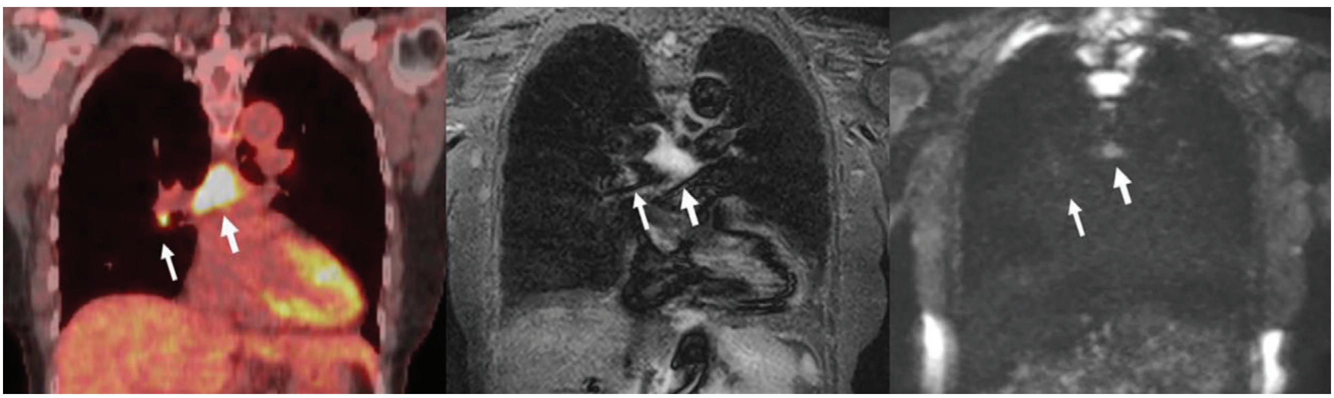

Figure 4: Images in 74-year-old man with lung cancer and right hilar and subcarinal lymph node metastases. Fluorine 18 fluorodeoxyglucose (FDG) PET/CT scan (left), short inversion time inversion-recovery turbo fast spin-echo image obtained with a 3-T system (middle), and diffusion-weighted (DW) image obtained with a fast spin-echo sequence from same system (right). PET/CT scan shows high uptake of FDG at right hilar (thin arrow) and subcarinal (thick arrow) lymph nodes. Short inversion time inversion-recovery fast spin-echo image demonstrates right hilar (thin arrow) and subcarinal (thick arrow) lymph nodes as areas of high signal intensity, although DW image shows only subcarinal lymph node (thick arrow) as high signal intensity and cannot visualize right hilar lymph node as high signal intensity (thin arrow). All methods could enable accurate diagnosis of N stage in this patient. In addition, PET/CT and short inversion time inversion-recovery fast spin-echo imaging could enable accurate diagnosis of lymph node metastases on a per-node basis. DW imaging could accurately depict subcarinal lymph node metastasis, but right hilar lymph node was determined to be a false-negative finding.

Table 2: Reported Diagnostic Performances of T Factor at MRI as Compared with CT

Study	Year	Field Strength (T)	Sequence	Image Analysis	MRI Accuracy (%)	CT Accuracy (%)
Webb et al (63)	1991	0.3 + 1.5	ECG-gated T1-and T2-weighted	Distinction between stage T0–T2 and T3–T4	73	78
Sakai et al (64)	1997	1.5	Free-breathing cine-GRASS	Chest wall invasion	76	68
Ohno et al (65)	2001	1.5	Dynamic ECG-triggered 3D GRE	Tumor invasion of pulmonary vessels	75–88	68–71
Tang et al (66)	2015	3.0	Breath-hold dynamic CE 2D GRE	T stage	82.2	84.4

Note.—CE = contrast enhanced, ECG = electrocardiogram, GRASS = gradient-recalled acquisition in the steady state, GRE = gradient recalled echo, 3D = three-dimensional, 2D = two-dimensional.

Table 3: Diagnostic Performance of N Factor of the TNM Staging System for MRI, CT, and FDG PET/CT

Study	Year	Field Strength (T)	Sequence	Reference Standard	MRI Accuracy (%)	CT Accuracy (%)	PET/CT Accuracy (%)
Takenaka et al (67)	2002	1.5	ECG-triggered T1-weighted TSE, STIR	Histologic findings	83 (T1WI), 96 (STIR)	83	NA
Ohno et al (68)	2004	1.5	STIR	Histologic findings	89	72	NA
Ohno et al (69)	2007	1.5	STIR	Histologic findings and/or follow-up	87.8 (qualitative), 92.2 (quantitative)	82.6 (qualitative), 83.5 (quantitative)	NA
Hasegawa et al (70)	2008	1.5	DWI	Histologic findings	95	NA	NA
Nomori et al (71)	2008	1.5	DWI	Histologic findings and/or follow-up	98	NA	96
Morikawa et al (72)	2009	1.5	STIR	Histologic findings	84.7 (qualitative), 84.7 (quantitative)	NA	80.3
Nakayama et al (73)	2010	1.5	DWI	Histologic findings	94	NA	NA
Usuda et al (74)	2011	1.5	T1-weighted SE, T2-weighted FSE, SS EPI SPAIR	Histologic findings	81	NA	71
Ohno et al (75)	2011	1.5	STIR, DWI	Histologic findings	84.4 (qualitative STIR), 82.8 (qualitative DWI),86.8 (quantitative STIR), 84.4 (quantitative DWI)	NA	83.6 (qualitative), 85.6 (quantitative)
Ohno et al (76)	2015	3	STIR FASE, EPI DWI, FASE DWI	Histologic findings	84.2 (STIR FASE), 76.8 (EPI DWI), 83.2 (FASE DWI)	NA	73.7
Usuda (77)	2015	1.5	SE T1-weighted, FSE T2-weighted, DWI	Histologic findings and/or follow-up	91	NA	48
Nomori (78)	2016	1.5	DWI	Histologic findings	75	NA	67
Peerlings et al (79)	2016	Mainly 1.5	DWI and STIR	Meta-analysis	NA	NA	NA

Note.—DWI = diffusion weighted imaging, ECG = electrocardiogram, EPI = echo-planar imaging, FASE = fast-advantage spin echo, FDG = fluorine 18 fluorodeoxyglucose, FSE = fast spin echo, NA = not applicable, SE = spin echo, SS = single shot, SPAIR = spectral attenuated inversion recovery, STIR = short inversion time inversion recovery.

study have improved the resolution and image quality of the MRI examinations (105). Advances in scanner hardware have resulted in improved interpolated resolution (0.7 × 0.7 × 1.0 mm vs 0.5 × 0.7 × 1.5 mm in Prospective Investigation of Pulmonary Em-

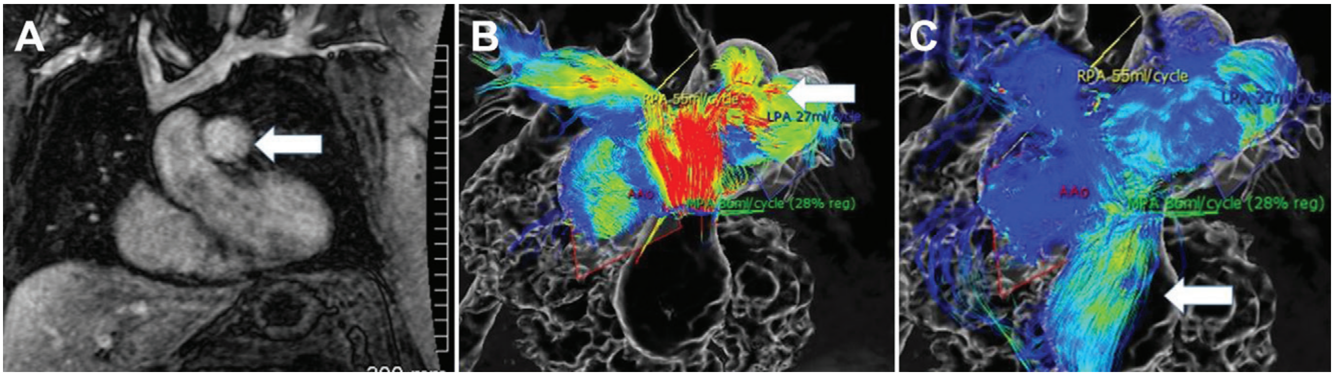

Figure 5: Images in 42-year-old woman with chronic pulmonary arterial hypertension from an atrial septal defect with pulmonary insufficiency. *A*, Coronal MR angiogram shows an enlarged pulmonary artery (arrow). *B*, Four-dimensional flow systolic phase pathlines from emitter plane at pulmonary valve shows rapid flow in red at the pulmonary trunk and turbulent (helical) flows in right and left (arrow) pulmonary arteries. *C*, Four-dimensional flow in diastolic phase shows lower velocity pulmonary insufficiency path lines in blue (arrow) from same emitter plane at pulmonary valve, with calculated regurgitant fraction of 28%.

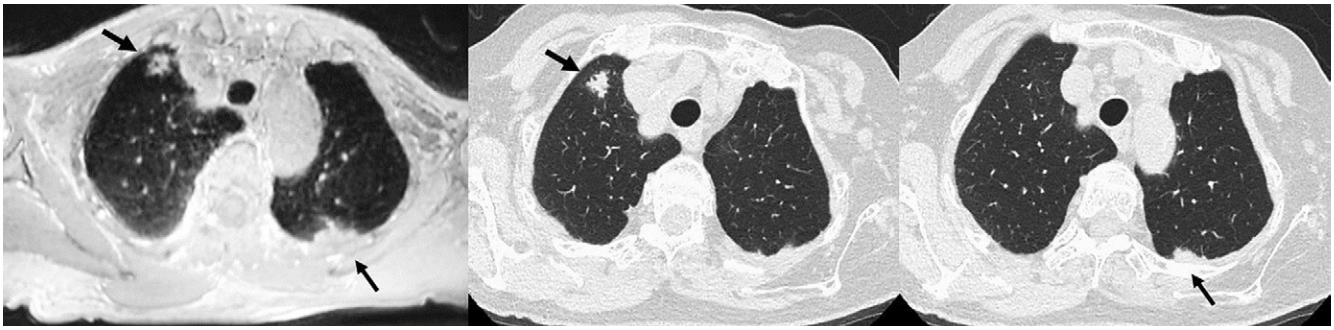

Figure 6: Images in 82-year-old man with solid nodules in lung apices. Pulmonary MRI scan with ultrashort echo time at 192 µsec (left) and thin-section CT scans with 1-mm-thick sections (center and right) show solid nodules (arrows) in the apices. Nodule diameters were 19 mm and 25 mm on MRI scan and 19 mm and 26 mm on thin-section CT scan. These nodules were diagnosed as invasive adenocarcinoma in right apex and squamous cell carcinoma in left apex.

bolism Diagnosis III), increased number of slices (140–160 vs 44 [101]), and a lower repetition time (2.9 msec vs 6.6 msec). The software changes also include the use of an auto calibrating k-space two-dimensional scheme for three-dimensional acquisition (106).

In conclusion, single-center data (n = 675) have shown that pulmonary MR angiography is similar to CT angiography for the primary evaluation of suspected pulmonary embolism. Confirmatory prospective, multicenter, outcomes-based trials comparing pulmonary MR angiography and CT angiography are needed.

Pulmonary parenchymal abnormalities.—Since 2000, advancements in MRI gradient systems and pulse sequences enabled the evaluation of lung parenchyma by using single-shot fast or turbo spin echo with and without half-Fourier acquisition, balanced steady-state free precession, and three-dimensional GRE with UTE less than 200 µsec (12,15,107–109). These techniques can increase the signal-to-noise ratio within the lung parenchyma (15). Steady-state free precession and three-dimensional GRE with UTE emerged for visualization of lung parenchymal structures in the 2010s (12,107–109). When compared with CT, three-dimensional GRE with UTE showed almost perfect agreement for imaging lung nodules or masses, ground-glass opacity, patchy opacity and consolidation, honeycombing and traction bronchiectasis, and substantial agreement in visualizing reticular opacity, emphysema, and bullae (109). Three-dimensional GRE with UTE is equally useful compared with thin-section CT for lung nodule detection and characterization (Figs 6–8) (54,110). Another application of this technique is the quantitative regional T2* measurement of the lung by direct T2* decay at three-dimensional GRE with UTEs for the assessment of lung microstructure and emphysema (111).

In conclusion, several studies suggest MRI may be comparable to CT in the detection of lung nodules, ground-glass opacity, consolidation, honeycombing, traction bronchiectasis, and reticular changes. However, the limited availability and investigational status of UTE proton pulse sequences have curtailed clinical adoption. Evidence from multicenter clinical trials is required for validation.

Investigational (Appropriate for Research Investigations and Mechanistic and Hypothesis-driven Research in Patients or Preclinical Studies)

Chronic obstructive pulmonary disease.—Chronic obstructive pulmonary disease (COPD) is the most common chronic respiratory illness in the world, and it is increasing in prevalence with decidedly poor prognosis and outcomes. Pulmonary function tests and CT currently serve as the established clinical tools for COPD evaluations and large-scale multicenter stud-

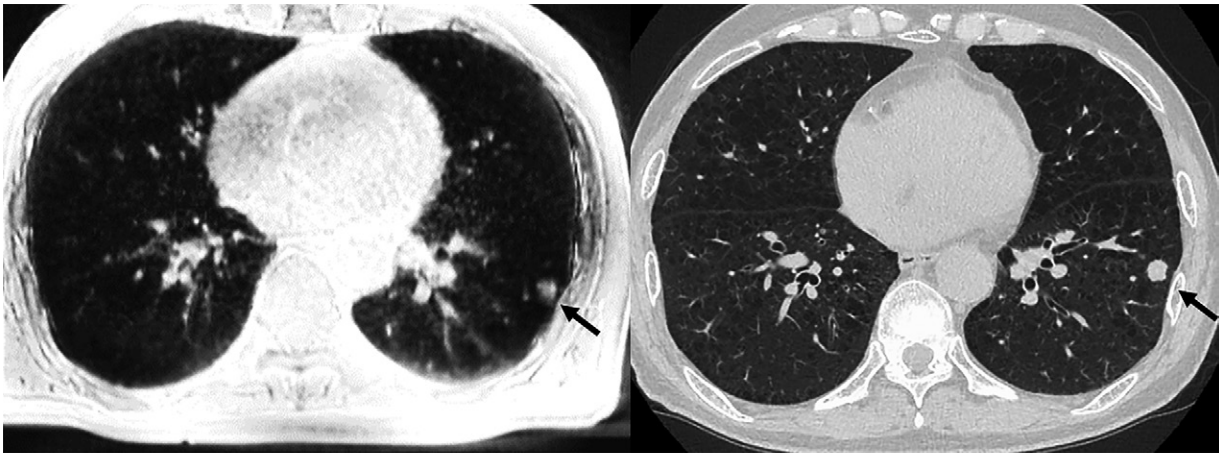

Figure 7: Images in 74-year-old man with solid lung nodule. Pulmonary MRI scan obtained with ultrashort echo time at 110 μsec (left) and thin-section CT scan obtained with 1-mm-thick sections (right) show solid nodule in left lower lobe (arrows). The nodule measures 14 mm on MRI scan and 15 mm on thin-section CT scan. This nodule was diagnosed as invasive adenocarcinoma.

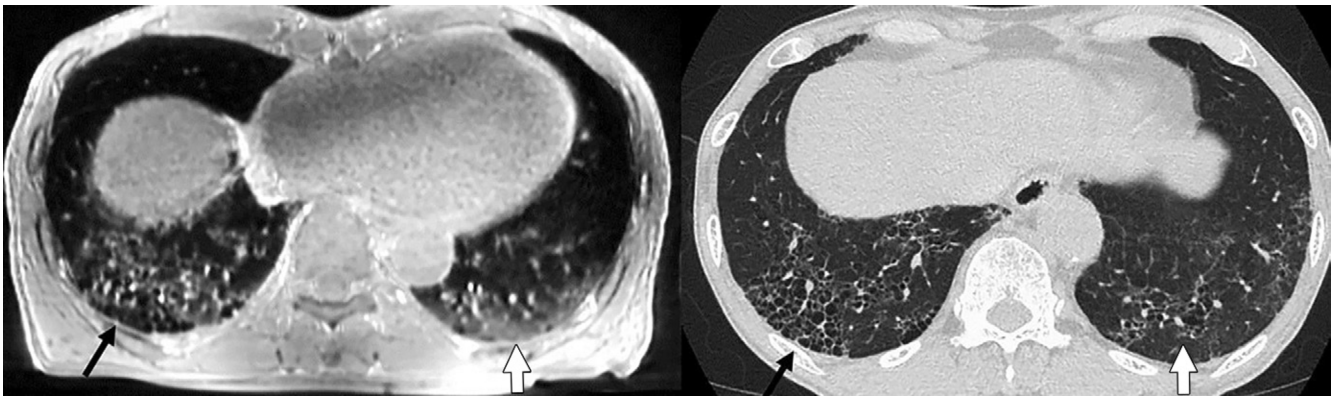

Figure 8: Images in 72-year-old man with usual interstitial pneumonia. Pulmonary MRI with ultra-short echo time at 192 μsec at end of tidal expiration by respiratory triggering (left) and thin-section CT at end full inspiration with 1 mm section thickness (right) shows honeycombing in the right lower lobe (black arrow) and reticulation in the left lower lobe (white arrow). Although honeycombing was demonstrated with good agreement, reticulation was demonstrated with difference due to different respiratory volumes.

ies (112). Several smaller COPD studies have employed MRI methods.

The first large-scale multi-institutional study involved a collaboration with the United Kingdom, Germany, and Denmark, the Polarized Helium Imaging of the Lung study (113). This prospective study compared hyperpolarized helium MRI and CT in nearly 200 patients with COPD and never-smokers. Using pulmonary function tests as a reference, regional analysis of hyperpolarized helium MRI and thin-section CT correctly categorized healthy volunteers in 100% and 97% and COPD in 42% and 69%, respectively. The apparent diffusion coefficients of hyperpolarized helium MRI better correlate with diffusing capacity of the lung for carbon monoxide than CT lung density (r = 0.59 vs r = 0.29) (113). The first evidence of hyperpolarized helium MRI utility in COPD was provided much earlier (114,115), and these findings opened the door to larger studies in patients and in those exposed to secondhand smoke (116). In one pilot hyperpolarized helium MRI study, increased ventilation defects and apparent diffusion coefficients were detected during a 2-year period in patients with COPD in whom forced expiratory volume in 1 second remained unchanged (117), underscoring the sensitivity of MRI to COPD abnormalities. In a larger COPD cohort study, hyperpolarized helium MRI apparent diffusion coefficient values were used to explain ventilation improvements after bronchodilator treatment (118). Moreover, in a comparison of CT, pulmonary function tests, and hyperpolarized helium MRI in a larger COPD cohort, only hyperpolarized helium MRI enabled the prediction of exacerbations in patients with mild to moderate COPD without previous exacerbations (119). Time-resolved hyperpolarized helium MRI was also exploited to directly visualize collateral ventilation in a small group (four of 10) of patients with COPD (120). DW hyperpolarized helium MRI has also helped detect subclinical emphysema in healthy smokers (121,122) with high sensitivity, although hyperpolarized xenon MRI b value acquisition methods can quantify mean alveolar dimensions in COPD (123) (Fig 9).

Quantitative perfusion MRI has also been employed in patients with COPD with correlation to CT and pulmonary function tests (124–128). In 144 participants, pulmonary microvascular blood flow was reduced in mild COPD compared with control participants who were smokers, independent of small airway disease at CT and gas trapping at pulmonary function

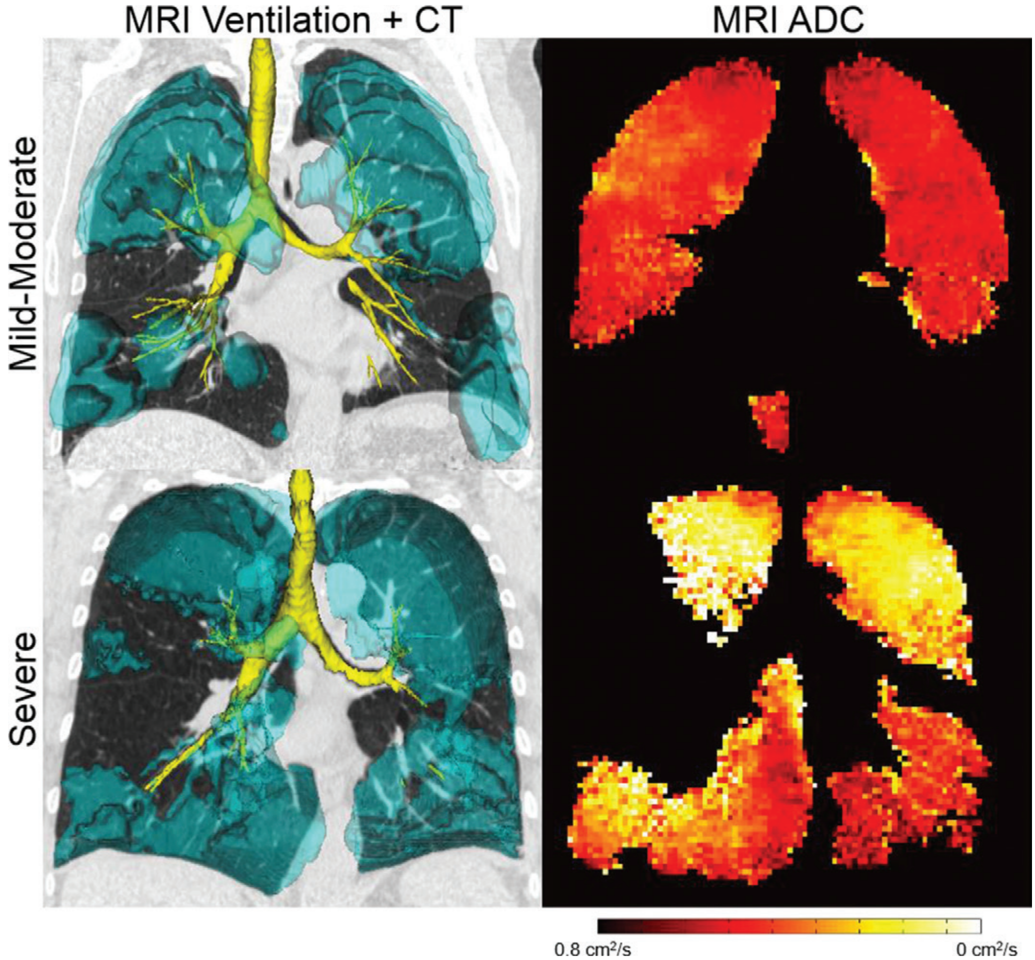

Figure 9: Images in 61-year-old man with mild to moderate chronic obstructive pulmonary disease (COPD) (top) and 61-year-old woman with severe COPD (bottom). Images on left are MRI ventilation scans coregistered to CT scans, and images on right are corresponding center slice MRI apparent diffusion coefficient maps. MRI ventilation (cyan) was volume rendered in three dimensions and coregistered to center-slice thoracic CT scan (gray scale) and three-dimensional rendered airway tree (yellow). The patient with mild to moderate COPD had forced expiratory volume in 1 second of 55% percentage predicted, ventilation defect percentage of 29%, and apparent diffusion coefficient of 0.36 cm^2/sec. The patient with severe COPD had forced expiratory volume in 1 second of 30% percentage predicted, ventilation defect percentage of 36%, and apparent diffusion coefficient of 0.54 cm^2/sec.

tests (126). Pulmonary microvascular blood flow at MRI was associated with signs of endothelial injury, including elevated endothelial microparticles and reduced circulating endothelial cells (127,128). In 79 participants, perfusion MRI was more sensitive to abnormalities among smokers with normal pulmonary function (129), and it helped distinguish patients among three phenotypes (130). In 15 patients with COPD, perfusion MRI helped evaluate acute exacerbations and postexacerbation improvements, showing that perfusion defects resolved after therapy (131). In a multicenter study of 160 patients with COPD, oxygen-enhanced pulmonary MRI showed functional derangements that distinguished patients similar to clinical severity staging (132). UTE MRI also showed reproducible signal intensity changes in the lung parenchyma, which were related to pulmonary function tests and CT measurements such as relative area of the density histogram less than or equal to –950 HU and forced expiratory volume in 1 second/forced vital capacity (133). Fluorine 19 MRI in patients with COPD has also been piloted with promising results (134,135). A noncontrast method for the assessment of ventilation and perfusion in patients with COPD has also been employed (Appendix E1 [online]) (136).

Only three relatively large-scale MRI studies of COPD have been reported: two multicenter trials in Europe, Japan, and South Korea (113,132) and a single-center Canadian study (137). Comparative studies between ^{3}He and ^{129}Xe indicate similar sensitivity to lung obstruction and emphysema (138–140). Clinical trials with multiple institutions using hyperpolarized xenon are under way.

*Asthma.—*Asthma is the most common chronic disease in children (141), and it is a leading cause of workplace absence in adults (142). Until recently, MRI has played a very limited role in the clinical assessment of asthma. However, CT has been used to measure functional air trapping (143), and the National Institutes of Health–funded Severe Asthma Research Program study also highlighted the utility of CT in understanding asthma severity (144).

Pulmonary MRI without exogenous contrast material, such as Fourier decomposition MRI (28), provides a method to

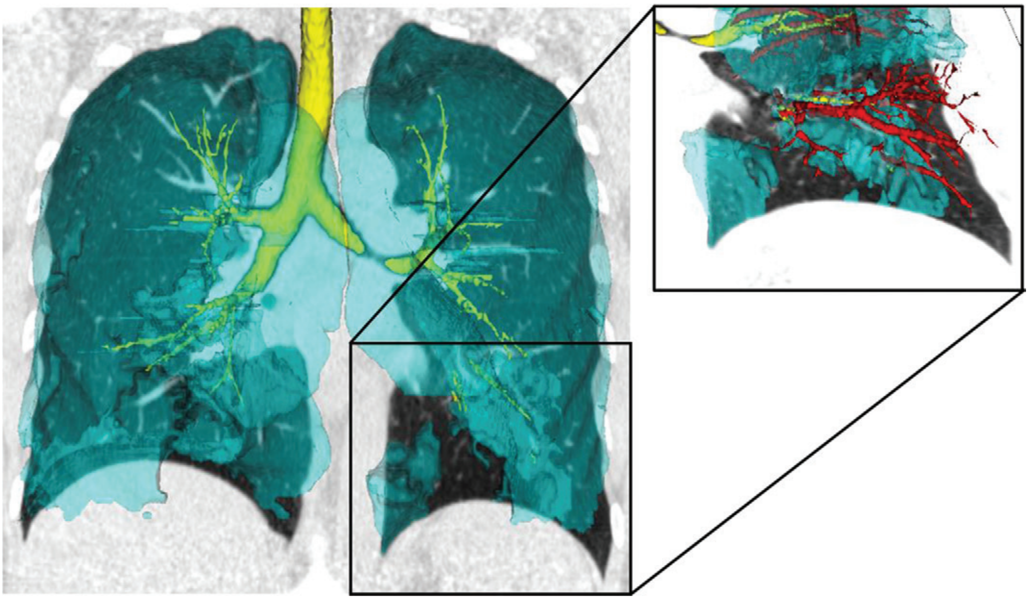

Figure 10: MRI ventilation image coregistered to CT scan in 41-year-old woman with asthma. MRI ventilation (cyan) was volume rendered in three dimensions and coregistered to center-slice thoracic CT scan (gray scale) and three-dimensional rendered airway tree (yellow). Zooming in on left lower lobe MRI ventilation defect with three-dimensional rendered pulmonary vasculature (red) reveals vascular pruning within ventilation defects. In this patient, the forced expiratory volume in 1 second was 60% percentage predicted, and ventilation defect percentage was 15%.

generate ventilation and perfusion maps in patients with asthma (145). In a similar manner, multivolume acquisitions (146), followed by quantification of signal intensities related to inhalation, provide ventilation heterogeneity maps in asthma.

Although MRI with intravenous gadolinium-based contrast agents has been used to generate quantitative lung perfusion information for direct comparison with pulmonary function test measurements, the vast majority of asthma MRI studies involve inhaled gas contrast hyperpolarized helium and hyperpolarized xenon methods that were pioneered by the team at the University of Virginia. These investigators provided the initial evidence of the utility of hyperpolarized helium ventilation MRI in patients with asthma (147–150). They were also the first to describe the spatial persistence of hyperpolarized helium MRI ventilation abnormalities in asthma (151,152) and the clinical relevance of these hyperpolarized helium MRI measures (153,154). Others have evaluated hyperpolarized helium MRI response to methacholine challenge and other triggers such as exercise (155) and treatment (148,156, 157). These studies focused on ventilation quantification, which can be automated by coregistration of ventilation volume and the thoracic cavity volume (158). More recently, the relationships of hyperpolarized MRI ventilation abnormalities with asthma control (159), eosinophilic inflammation (160), and mucus plugs (161) were ascertained, all of which are relevant for the clinical management of asthma (Fig 10).

Interstitial lung disease.—Recent developments in UTE hydrogen 1 MRI (12) have shown comparable diagnostic accuracy to CT (109,162,163) in interstitial lung disease (Fig 8). T1 values of fibrotic lung parenchyma are longer than those of emphysematous lung parenchyma and are influenced by lung volume (164), while ground-glass opacity, reticulation, and honeycombing have different T2 relaxation times in nonspecific interstitial pneumonia or usual interstitial pneumonia (165). MR elastography has revealed increased lung stiffness in 15 patients with interstitial lung disease (166).

Oxygen-enhanced proton MRI of interstitial lung disease has shown enhancement changes in patients versus healthy controls (167–170). Hyperpolarized xenon MRI spectroscopy revealed reduced signal from red blood cells compared with tissue in idiopathic pulmonary fibrosis versus healthy volunteers (171). Hyperpolarized xenon MRI showed good correlations with pulmonary function tests (172). In patients with idiopathic pulmonary fibrosis, the ratio of hyperpolarized xenon MRI red blood cells–to–tissue barrier is more sensitive to change than forced vital capacity and diffusing capacity of the lung for carbon monoxide (173), although hyperpolarized xenon and hyperpolarized helium apparent diffusion coefficients are more sensitive to acinar microstructural changes that correlate with the Likert fibrosis score derived from CT (138,174). Early and late T1 contrast enhancement features may help differentiate inflammation from fibrotic-predominant pathology, as shown in a biopsy study that classified 26 patients with usual interstitial pneumonia as inflammation or fibrosis predominant (175).

Cost-effectiveness and Timeliness of Lung MRI

MRI is associated with cost, complexity, and difficulty in reading. Few publications are available regarding *(a)* cost-effectiveness data to support clinical use, to our knowledge, and *(b)* MRI timeliness (ie, time to complete the examination after ordering) compared with CT. More studies on the cost-effectiveness of pulmonary MRI and its timeliness are needed, particularly for children with chronic disease in need of longitudinal follow-up imaging (eg, patients with CF and adults in lung cancer screening programs) (176). Recently, Allen et al (177) reported that MRI has a near equivalent life expectancy benefit and superior cost-effectiveness compared with low-dose CT in a Markov model of lung cancer screening. To our knowledge, no publications show data of the timeliness of lung MRI examinations.

Summary and Future Directions

Until recently, the clinical use of pulmonary MRI has been limited. However, advanced methods are expanding opportunities to exploit the advantages of MRI for the evaluation of several common lung disorders. MRI helps visualize lung structural and functional abnormalities without ionizing radiation, making state-of-the-art MRI techniques an alternative to CT, particularly for pediatric patients, women of childbearing age, pregnant women, and patients requiring serial follow-up imaging where radiation burden is an issue. A clinically relevant example is the use of proton MRI in the serial imaging of children with CF. However, proton MRI pulse sequences are not universally accessible beyond specialist or research centers, so they remain underused for lung imaging. To maximize the potential of MRI to improve patient care, vendors and developers must ensure that more effective pulse sequences and measurements are more widely and easily available. The current roadblocks that stymie widespread adoption need to be addressed.

Although CT will remain the principal imaging tool for routine pulmonary imaging examinations, including in the pediatric population, MRI has either emerged as the clinical standard or has shown enormous potential to change clinical care for certain patients and indications. In addition, the unique information these MRI tools provide can be used for mechanistic, hypothesis-driven research in patients and preclinical models. Prospective and randomized multicenter trials should be conducted to directly compare MRI with conventional clinical approaches and imaging for the most promising or most burdensome pulmonary diseases. The results of such trials, along with continued improvements in pulmonary MRI methods, will likely necessitate future updated modifications in the recommendations proposed here.

Acknowledgments: We thank the librarians Myung Ah Shim, BA, and Jaero Park, MS, for their dedicated support in manuscript formatting. Both librarians work at the Samsung Medical Information and Media Services of Samsung Medical Center in Seoul, South Korea.

Author contributions: Guarantors of integrity of entire study, H.H., Y.O.; study concepts/study design or data acquisition or data analysis/interpretation, all authors; manuscript drafting or manuscript revision for important intellectual content, all authors; approval of final version of submitted manuscript, all authors; agrees to ensure any questions related to the work are appropriately resolved, all authors; literature research, H.H., Y.O., W.B.G., G.P., B.M., K.S.L., J.R.M., J.M.W., E.J.R.v.B., M.L.S., H.U.K.; clinical studies, H.H., J.R.M., H.U.K.; experimental studies, J.R.M.; statistical analysis, XXX; and manuscript editing, H.H., Y.O., W.B.G., G.P., B.M., K.S.L., T.A.A., J.R.M., J.B.S., J.M.W., E.J.R.v.B., M.L.S., H.U.K.

K.S.L. developed and implemented the systemic search strategy. D.A.L. advised on the systemic search. All authors participated in the literature search. H.H., Y.O., W.B.G., G.P., B.M., K.S.L., D.A.L., J.M.W., E.J.R.v.B., M.L.S., and H.U.K. created the first draft of the Review. All authors critically reviewed the manuscript and approved the final version, taking accountability for the work. The Document Development and Oversight Committee and Executive Committee of the Fleischner Society approved the manuscript before submission to *Radiology*.

Disclosures of Conflicts of Interest: **H.H.** Activities related to the present article: disclosed no relevant relationships. Activities not related to the present article: is a consultant for Mitsubishi Chemical; has grants/grants pending with Canon Medical and Konica Minolta; receives payment from Canon Medical for serving on medical advisory board. Other relationships: disclosed no relevant relationships. **Y.O.** Activities related to the present article: institution received research grant from Canon Medical Systems. Activities not related to the present article: has grants/grants pending with Daiichi Sankyo. Other relationships: disclosed no relevant relationships. **W.B.G.** Activities related to the present article: disclosed no relevant relationships. Activities not related to the present article: is a consultant for Imbio; has grants/grants pending with Siemens Medical Solutions USA. Other relationships: disclosed no relevant relationships. **G.P.** disclosed no relevant relationships. **B.M.** Activities related to the present article: disclosed no relevant relationships. Activities not related to the present article: has a consultancy agreement with Milli-Kelvin Technologies; has grants/grants pending; has patents (planned, pending, or issued); receives royalties. Other relationships: disclosed no relevant relationships. **K.S.L.** disclosed no relevant relationships. **T.A.A.** Activities related to the present article: institution received grant from National Institutes of Health. Activities not related to the present article: is a consultant for Vertex; receives payment for lectures, including service on speakers bureaus, from Philips; receives payment from Philips for development of educational presentations. Other relationships: disclosed no relevant relationships. **D.A.L.** disclosed no relevant relationships. **J.R.M.** Activities related to the present article: disclosed no relevant relationships. Activities not related to the present article: receives payment for lectures, including service on speakers bureaus, from Siemens Healthineers. Other relationships: disclosed no relevant relationships. **J.B.S.** disclosed no relevant relationships. **J.M.W.** disclosed no relevant relationships. **E.J.R.v.B.** Activities related to the present article: disclosed no relevant relationships. Activities not related to the present article: receives payment for board membership from Aidence, Imbio, and QCTIS; is a consultant for InHealth and Mentholatum. Other relationships: disclosed no relevant relationships. **M.L.S.** Activities related to the present article: disclosed no relevant relationships. Activities not related to the present article: disclosed no relevant relationships. Other relationships: is a shareholder in HealthMyne, Stemina Biomarker Discovery, and X-Vac. **H.U.K.** Activities related to the present article: disclosed no relevant relationships. Activities not related to the present article: has grants/grants pending with Siemens, Philips, and Bayer; receives payment for lectures, including service on speakers bureaus, from Philips, Boehringer Ingelheim, MSD, and Astra Zeneca. Other relationships: disclosed no relevant relationships.

References

1. Cutillo AG. Application of magnetic resonance to the study of lung. Armonk, NY: Futura, 1996.
2. Morris AH, Blatter DD, Case TA, et al. A new nuclear magnetic resonance property of lung. J Appl Physiol (1985) 1985;58(3):759–762.
3. Case TA, Durney CH, Ailion DC, Cutillo AG, Morris AH. A mathematical model of diamagnetic line broadening in lung tissue and similar heterogeneous systems: Calculations and measurements. J Magn Reason (1969) 1987;73(2):304–314.
4. Durney CH, Bertolina J, Ailion DC, et al. Calculation and interpretation of inhomogenous line broadening in models of lungs and other heterogenous structures. J Magn Reason (1969) 1989;85(3):554–570.
5. Bertolina JA, Durney CH, Ailion DC, Cutillo AG, Morris AH, Goodrich KC. Experimental verification of inhomogenous line-broadening calculations in lung models and other inhomogenous structures. J Magn Reson (1969) 1992;99(1):161–169.
6. Cutillo AG, Ganesan K, Ailion DC, et al. Alveolar air-tissue interface and nuclear magnetic resonance behavior of lung. J Appl Physiol (1985) 1991;70(5):2145–2154.
7. Bergin CJ, Pauly JM, Macovski A. Lung parenchyma: projection reconstruction MR imaging. Radiology 1991;179(3):777–781.
8. Bergin CJ, Glover GH, Pauly JM. Lung parenchyma: magnetic susceptibility in MR imaging. Radiology 1991;180(3):845–848.
9. Bergin CJ, Noll DC, Pauly JM, Glover GH, Macovski A. MR imaging of lung parenchyma: a solution to susceptibility. Radiology 1992;183(3):673–676.
10. Pauly JM, Conolly SM, Nishimura DG, Macovski A. Slice-selective excitation for very short T2 species [abstr]. In: Book of abstracts: Society of Magnetic Resonance in Medicine 1989. Berkeley, Calif: Society of Magnetic Resonance in Medicine, 1989; 28.
11. Glover GH, Pauly JM, Bradshaw KM. Boron-11 imaging with a three-dimensional reconstruction method. J Magn Reson Imaging 1992;2(1):47–52.
12. Johnson KM, Fain SB, Schiebler ML, Nagle S. Optimized 3D ultrashort echo time pulmonary MRI. Magn Reson Med 2013;70(5):1241–1250.
13. Mayo JR, MacKay A, Müller NL. MR imaging of the lungs: value of short TE spin-echo pulse sequences. AJR Am J Roentgenol 1992;159(5):951–956.
14. Alsop DC, Hatabu H, Bonnet M, Listerud J, Gefter W. Multi-slice, breath-hold imaging of the lung with submillisecond echo times. Magn Reson Med 1995;33(5):678–682.
15. Hatabu H, Gaa J, Tadamura E, et al. MR imaging of pulmonary parenchyma with a half-Fourier single-shot turbo spin-echo (HASTE) sequence. Eur J Radiol 1999;29(2):152–159.
16. Hatabu H, Gefter WB, Kressel HY, Axel L, Lenkinski RE. Pulmonary vasculature: high-resolution MR imaging. Work in progress. Radiology 1989;171(2):391–395.
17. Gefter WB, Hatabu H, Dinsmore BJ, et al. Pulmonary vascular cine MR imaging: a noninvasive approach to dynamic imaging of the pulmonary circulation. Radiology 1990;176(3):761–770.
18. Albert MS, Cates GD, Driehuys B, et al. Biological magnetic resonance imaging using laser-polarized 129Xe. Nature 1994;370(6486):199–201.

19. Kauczor HU, Hofmann D, Kreitner KF, et al. Normal and abnormal pulmonary ventilation: visualization at hyperpolarized He-3 MR imaging. Radiology 1996;201(2):564–568.
20. MacFall JR, Charles HC, Black RD, et al. Human lung air spaces: potential for MR imaging with hyperpolarized He-3. Radiology 1996;200(2):553–558.
21. Hatabu H, Gaa J, Kim D, Li W, Prasad PV, Edelman RR. Pulmonary perfusion: qualitative assessment with dynamic contrast-enhanced MRI using ultra-short TE and inversion recovery turbo FLASH. Magn Reson Med 1996;36(4):503–508.
22. Hatabu H, Tadamura E, Levin DL, et al. Quantitative assessment of pulmonary perfusion with dynamic contrast-enhanced MRI. Magn Reson Med 1999;42(6):1033–1038.
23. Levin DL, Chen Q, Zhang M, Edelman RR, Hatabu H. Evaluation of regional pulmonary perfusion using ultrafast magnetic resonance imaging. Magn Reson Med 2001;46(1):166–171.
24. Ohno Y, Hatabu H, Murase K, et al. Quantitative assessment of regional pulmonary perfusion in the entire lung using three-dimensional ultrafast dynamic contrast-enhanced magnetic resonance imaging: Preliminary experience in 40 subjects. J Magn Reson Imaging 2004;20(3):353–365.
25. Edelman RR, Hatabu H, Tadamura E, Li W, Prasad PV. Noninvasive assessment of regional ventilation in the human lung using oxygen-enhanced magnetic resonance imaging. Nat Med 1996;2(11):1236–1239.
26. Hatabu H, Tadamura E, Chen Q, et al. Pulmonary ventilation: dynamic MRI with inhalation of molecular oxygen. Eur J Radiol 2001;37(3):172–178.
27. Ohno Y, Hatabu H, Takenaka D, Van Cauteren M, Fujii M, Sugimura K. Dynamic oxygen-enhanced MRI reflects diffusing capacity of the lung. Magn Reson Med 2002;47(6):1139–1144.
28. Bauman G, Puderbach M, Deimling M, et al. Non-contrast-enhanced perfusion and ventilation assessment of the human lung by means of fourier decomposition in proton MRI. Magn Reson Med 2009;62(3):656–664.
29. Puderbach M, Eichinger M, Haeselbarth J, et al. Assessment of morphological MRI for pulmonary changes in cystic fibrosis (CF) patients: comparison to thin-section CT and chest x-ray. Invest Radiol 2007;42(10):715–725.
30. Wielpütz MO, Puderbach M, Kopp-Schneider A, et al. Magnetic resonance imaging detects changes in structure and perfusion, and response to therapy in early cystic fibrosis lung disease. Am J Respir Crit Care Med 2014;189(8):956–965.
31. Roach DJ, Crémillieux Y, Fleck RJ, et al. Ultrashort Echo-Time Magnetic Resonance Imaging Is a Sensitive Method for the Evaluation of Early Cystic Fibrosis Lung Disease. Ann Am Thorac Soc 2016;13(11):1923–1931.
32. Ciet P, Tiddens HA, Wielopolski PA, et al. Magnetic resonance imaging in children: common problems and possible solutions for lung and airways imaging. Pediatr Radiol 2015;45(13):1901–1915.
33. Failo R, Wielopolski PA, Tiddens HA, Hop WC, Mucelli RP, Lequin MH. Lung morphology assessment using MRI: a robust ultra-short TR/TE 2D steady state free precession sequence used in cystic fibrosis patients. Magn Reson Med 2009;61(2):299–306.
34. Eichinger M, Optazaite DE, Kopp-Schneider A, et al. Morphologic and functional scoring of cystic fibrosis lung disease using MRI. Eur J Radiol 2012;81(6):1321–1329.
35. Hopkins SR, Wielpütz MO, Kauczor H-U. Imaging lung perfusion. J Appl Physiol (1985) 2012;113(2):328–339.
36. Stahl M, Wielpütz MO, Graeber SY, et al. Comparison of Lung Clearance Index and Magnetic Resonance Imaging for Assessment of Lung Disease in Children with Cystic Fibrosis. Am J Respir Crit Care Med 2017;195(3):349–359.
37. Santyr G, Kanhere N, Morgado F, Rayment JH, Ratjen F, Couch MJ. Hyperpolarized Gas Magnetic Resonance Imaging of Pediatric Cystic Fibrosis Lung Disease. Acad Radiol 2019;26(3):344–354.
38. Wielpütz MO, von Stackelberg O, Stahl M, et al. Multicentre standardisation of chest MRI as radiation-free outcome measure of lung disease in young children with cystic fibrosis. J Cyst Fibros 2018;17(4):518–527.
39. Altes TA, Johnson M, Fidler M, et al. Use of hyperpolarized helium-3 MRI to assess response to ivacaftor treatment in patients with cystic fibrosis. J Cyst Fibros 2017;16(2):267–274.
40. van Beek EJ, Hill C, Woodhouse N, et al. Assessment of lung disease in children with cystic fibrosis using hyperpolarized 3-Helium MRI: comparison with Shwachman score, Chrispin-Norman score and spirometry. Eur Radiol 2007;17(4):1018–1024.
41. Marshall H, Horsley A, Taylor CJ, et al. Detection of early subclinical lung disease in children with cystic fibrosis by lung ventilation imaging with hyperpolarised gas MRI. Thorax 2017;72(8):760–762.
42. Woodhouse N, Wild JM, van Beek EJ, Hoggard N, Barker N, Taylor CJ. Assessment of hyperpolarized 3He lung MRI for regional evaluation of interventional therapy: a pilot study in pediatric cystic fibrosis. J Magn Reson Imaging 2009;30(5):981–988.
43. Smith L, Marshall H, Aldag I, et al. Longitudinal Assessment of Children with Mild Cystic Fibrosis Using Hyperpolarized Gas Lung Magnetic Resonance Imaging and Lung Clearance Index. Am J Respir Crit Care Med 2018;197(3):397–400.
44. Altes TA, Meyer CH, Mata JF, et al. Hyperpolarized helium-3 magnetic resonance lung imaging of non-sedated infants and young children: a proof-of-concept study. Clin Imaging 2017;45:105–110.
45. Thomen RP, Walkup LL, Roach DJ, Cleveland ZI, Clancy JP, Woods JC. Hyperpolarized ^{129}Xe for investigation of mild cystic fibrosis lung disease in pediatric patients. J Cyst Fibros 2017;16(2):275–282.
46. Kanhere N, Couch MJ, Kowalik K, et al. Correlation of Lung Clearance Index with Hyperpolarized ^{129}Xe Magnetic Resonance Imaging in Pediatric Subjects with Cystic Fibrosis. Am J Respir Crit Care Med 2017;196(8):1073–1075.
47. Couch MJ, Thomen R, Kanhere N, et al. A two-center analysis of hyperpolarized ^{129}Xe lung MRI in stable pediatric cystic fibrosis: Potential as a biomarker for multi-site trials. J Cyst Fibros 2019;18(5):728–733.
48. Rayment JH, Couch MJ, McDonald N, et al. Hyperpolarised ^{129}Xe magnetic resonance imaging to monitor treatment response in children with cystic fibrosis. Eur Respir J 2019;53(5):1802188.
49. Bauman G, Puderbach M, Heimann T, et al. Validation of Fourier decomposition MRI with dynamic contrast-enhanced MRI using visual and automated scoring of pulmonary perfusion in young cystic fibrosis patients. Eur J Radiol 2013;82(12):2371–2377.
50. Triphan SM, Jobst BJ, Breuer FA, et al. Echo time dependence of observed T1 in the human lung. J Magn Reson Imaging 2015;42(3):610–616.
51. Veldhoen S, Weng AM, Knapp J, et al. Self-gated Non-Contrast-enhanced Functional Lung MR Imaging for Quantitative Ventilation Assessment in Patients with Cystic Fibrosis. Radiology 2017;283(1):242–251.
52. Koyama H, Ohno Y, Kono A, et al. Quantitative and qualitative assessment of non-contrast-enhanced pulmonary MR imaging for management of pulmonary nodules in 161 subjects. Eur Radiol 2008;18(10):2120–2131.
53. Cieszanowski A, Lisowska A, Dabrowska M, et al. MR Imaging of Pulmonary Nodules: Detection Rate and Accuracy of Size Estimation in Comparison to Computed Tomography. PLoS One 2016;11(6):e0156272.
54. Ohno Y, Koyama H, Yoshikawa T, et al. Standard-, Reduced-, and No-Dose Thin-Section Radiologic Examinations: Comparison of Capability for Nodule Detection and Nodule Type Assessment in Patients Suspected of Having Pulmonary Nodules. Radiology 2017;284(2):562–573.
55. Yi CA, Jeon TY, Lee KS, et al. 3-T MRI: usefulness for evaluating primary lung cancer and small nodules in lobes not containing primary tumors. AJR Am J Roentgenol 2007;189(2):386–392.
56. Meier-Schroers M, Homsi R, Gieseke J, Schild HH, Thomas D. Lung cancer screening with MRI: Evaluation of MRI for lung cancer screening by comparison of LDCT- and MRI-derived Lung-RADS categories in the first two screening rounds. Eur Radiol 2019;29(2):898–905.
57. Jiang W, Ong F, Johnson KM, et al. Motion robust high resolution 3D free-breathing pulmonary MRI using dynamic 3D image self-navigator. Magn Reson Med 2018;79(6):2954–2967.
58. Ohno Y, Nishio M, Koyama H, et al. Dynamic contrast-enhanced CT and MRI for pulmonary nodule assessment. AJR Am J Roentgenol 2014;202(3):515–529.
59. Li B, Li Q, Chen C, Guan Y, Liu S. A systematic review and meta-analysis of the accuracy of diffusion-weighted MRI in the detection of malignant pulmonary nodules and masses. Acad Radiol 2014;21(1):21–29.
60. Ohno Y, Koyama H, Takenaka D, et al. Dynamic MRI, dynamic multidetector-row computed tomography (MDCT), and coregistered 2-[fluorine-18]-fluoro-2-deoxy-D-glucose-positron emission tomography (FDG-PET)/CT: comparative study of capability for management of pulmonary nodules. J Magn Reson Imaging 2008;27(6):1284–1295.
61. Ohno Y, Nishio M, Koyama H, et al. Solitary pulmonary nodules: Comparison of dynamic first-pass contrast-enhanced perfusion area-detector CT, dynamic first-pass contrast-enhanced MR imaging, and FDG PET/CT. Radiology 2015;274(2):563–575.
62. Basso Dias A, Zanon M, Altmayer S, et al. Fluorine 18-FDG PET/CT and Diffusion-weighted MRI for Malignant versus Benign Pulmonary Lesions: A Meta-Analysis. Radiology 2019;290(2):525–534.
63. Webb WR, Gatsonis C, Zerhouni EA, et al. CT and MR imaging in staging non-small cell bronchogenic carcinoma: report of the Radiologic Diagnostic Oncology Group. Radiology 1991;178(3):705–713.
64. Sakai S, Murayama S, Murakami J, Hashiguchi N, Masuda K. Bronchogenic carcinoma invasion of the chest wall: evaluation with dynamic cine MRI during breathing. J Comput Assist Tomogr. 1997; 21(4):595-600.
65. Ohno Y, Adachi S, Motoyama A, et al. Multiphase ECG-triggered 3D contrast-enhanced MR angiography: utility for evaluation of hilar and mediastinal invasion of bronchogenic carcinoma. J Magn Reson Imaging 2001;13(2):215–224.

66. Tang W, Wu N, OuYang H, Huang Y, Liu L, Li M. The presurgical T staging of non-small cell lung cancer: efficacy comparison of 64-MDCT and 3.0 T MRI. Cancer Imaging. 2015;15(1):14.
67. Takenaka D, Ohno Y, Hatabu H, et al. Differentiation of metastatic versus non-metastatic mediastinal lymph nodes in patients with non-small cell lung cancer using respiratory-triggered short inversion time inversion recovery (STIR) turbo spin-echo MR imaging. Eur J Radiol. 2002 Dec;44(3):216-24.
68. Ohno Y, Hatabu H, Takenaka D, et al. Metastases in mediastinal and hilar lymph nodes in patients with non-small cell lung cancer: quantitative and qualitative assessment with STIR turbo spin-echo MR imaging. Radiology. 2004; 231(3):872-879.
69. Ohno Y, Koyama H, Nogami M, et al. STIR turbo SE MR imaging vs. coregistered FDG-PET/CT: quantitative and qualitative assessment of N-stage in non-small-cell lung cancer patients. J Magn Reson Imaging. 2007; 26(4):1071-1080.
70. Hasegawa I, Boiselle PM, Kuwabara K, Sawafuji M, Sugiura H. Mediastinal lymph nodes in patients with non-small cell lung cancer: preliminary experience with diffusion-weighted MR imaging. J Thorac Imaging. 2008; 23(3): 157-161.
71. Nomori H, Mori T, Ikeda K, et al. Diffusion-weighted magnetic resonance imaging can be used in place of positron emission tomography for N staging of non-small cell lung cancer with fewer false-positive results. J Thorac Cardiovasc Surg. 2008; 135(4): 816-822.
72. Morikawa M, Demura Y, Ishizaki T, et al. The effectiveness of 18F-FDG PET/CT combined with STIR MRI for diagnosing nodal involvement in the thorax. J Nucl Med. 2009 Jan;50(1):81-7.
73. Nakayama J, Miyasaka K, Omatsu T, et al. Metastases in mediastinal and hilar lymph nodes in patients with non-small cell lung cancer: quantitative assessment with diffusion-weighted magnetic resonance imaging and apparent diffusion coefficient. J Comput Assist Tomogr. 2010; 34(1): 1-8.
74. Usuda K, Zhao XT, Sagawa M, et al. Diffusion-weighted imaging is superior to positron emission tomography in the detection and nodal assessment of lung cancers. Ann Thorac Surg. 2011; 91(6): 1689-1695.
75. Ohno Y, Koyama H, Yoshikawa T, et al. N stage disease in patients with non-small cell lung cancer: efficacy of quantitative and qualitative assessment with STIR turbo spin-echo imaging, diffusion-weighted MR imaging, and fluorodeoxyglucose PET/CT. Radiology 2011;261(2):605–615.
76. Ohno Y, Koyama H, Yoshikawa T, et al. Diffusion-weighted MR imaging using FASE sequence for 3T MR system: Preliminary comparison of capability for N-stage assessment by means of diffusion-weighted MR imaging using EPI sequence, STIR FASE imaging and FDG PET/CT for non-small cell lung cancer patients. Eur J Radiol. 2015; 84(11):2321-31.
77. Usuda K, Maeda S, Motono N, et al. Diagnostic Performance of Diffusion-Weighted Imaging for Multiple Hilar and Mediastinal Lymph Nodes with FDG Accumulation. Asian Pac J Cancer Prev. 2015; 16(15): 6401-6406.
78. Nomori H, Cong Y, Sugimura H, Kato Y. Diffusion-weighted imaging can correctly identify false-positive lymph nodes on positron emission tomography in non-small cell lung cancer. Surg Today. 2016; 46(10): 1146-1151.
79. Peerlings J, Troost EG, Nelemans PJ, et al. The Diagnostic Value of MR Imaging in Determining the Lymph Node Status of Patients with Non-Small Cell Lung Cancer: A Meta-Analysis. Radiology 2016;281(1): 86–98.
80. Kim YN, Yi CA, Lee KS, et al. A proposal for combined MRI and PET/CT interpretation criteria for preoperative nodal staging in non-small-cell lung cancer. Eur Radiol 2012;22(7):1537–1546.
81. Yi CA, Shin KM, Lee KS, et al. Non-small cell lung cancer staging: efficacy comparison of integrated PET/CT versus 3.0-T whole-body MR imaging. Radiology 2008;248(2):632–642.
82. Yi CA, Lee KS, Lee HY, et al. Coregistered whole body magnetic resonance imaging-positron emission tomography (MRI-PET) versus PET-computed tomography plus brain MRI in staging resectable lung cancer: comparisons of clinical effectiveness in a randomized trial. Cancer 2013;119(10):1784–1791.
83. Schaarschmidt BM, Grueneisen J, Metzenmacher M, et al. Thoracic staging with ^{18}F-FDG PET/MR in non-small cell lung cancer : does it change therapeutic decisions in comparison to ^{18}F-FDG PET/CT? Eur Radiol 2017;27(2):681–688.
84. Lee SM, Goo JM, Park CM, et al. Preoperative staging of non-small cell lung cancer: prospective comparison of PET/MR and PET/CT. Eur Radiol 2016;26(11):3850–3857.
85. Galiè N, Humbert M, Vachiery JL, et al. 2015 ESC/ERS Guidelines for the diagnosis and treatment of pulmonary hypertension: The Joint Task Force for the Diagnosis and Treatment of Pulmonary Hypertension of the European Society of Cardiology (ESC) and the European Respiratory Society (ERS): Endorsed by: Association for European Paediatric and Congenital Cardiology (AEPC), International Society for Heart and Lung Transplantation (ISHLT). Eur Heart J 2016;37(1):67–119.
86. Kiely DG, Levin D, Hassoun P, et al. EXPRESS: Statement on imaging and pulmonary hypertension from the Pulmonary Vascular Research Institute (PVRI). Pulm Circ 2019. 10.1177/2045894019841990. Published online March 18, 2019.
87. Rajaram S, Swift AJ, Telfer A, et al. 3D contrast-enhanced lung perfusion MRI is an effective screening tool for chronic thromboembolic pulmonary hypertension: results from the ASPIRE Registry. Thorax 2013;68(7):677–678.
88. Johns CS, Swift AJ, Rajaram S, et al. Lung perfusion: MRI vs. SPECT for screening in suspected chronic thromboembolic pulmonary hypertension. J Magn Reson Imaging 2017;46(6):1693–1697.
89. Swift AJ, Wild JM, Nagle SK, et al. Quantitative magnetic resonance imaging of pulmonary hypertension: a practical approach to the current state of the art. J Thorac Imaging 2014;29(2):68–79.
90. van de Veerdonk MC, Kind T, Marcus JT, et al. Progressive right ventricular dysfunction in patients with pulmonary arterial hypertension responding to therapy. J Am Coll Cardiol 2011;58(24):2511–2519.
91. Peacock AJ, Crawley S, McLure L, et al. Changes in right ventricular function measured by cardiac magnetic resonance imaging in patients receiving pulmonary arterial hypertension-targeted therapy: the EURO-MR study. Circ Cardiovasc Imaging 2014;7(1):107–114.
92. van Wolferen SA, van de Veerdonk MC, Mauritz GJ, et al. Clinically significant change in stroke volume in pulmonary hypertension. Chest 2011;139(5):1003–1009.
93. van Wolferen SA, Marcus JT, Boonstra A, et al. Prognostic value of right ventricular mass, volume, and function in idiopathic pulmonary arterial hypertension. Eur Heart J 2007;28(10):1250–1257.
94. Ohno Y, Hatabu H, Murase K, et al. Primary pulmonary hypertension: 3D dynamic perfusion MRI for quantitative analysis of regional pulmonary perfusion. AJR Am J Roentgenol 2007;188(1):48–56.
95. Ohno Y, Koyama H, Nogami M, et al. Dynamic perfusion MRI: capability for evaluation of disease severity and progression of pulmonary arterial hypertension in patients with connective tissue disease. J Magn Reson Imaging 2008;28(4):887–899.
96. Ohno Y, Koyama H, Yoshikawa T, et al. Contrast-enhanced multidetector-row computed tomography vs. Time-resolved magnetic resonance angiography vs. contrast-enhanced perfusion MRI: assessment of treatment response by patients with inoperable chronic thromboembolic pulmonary hypertension. J Magn Reson Imaging 2012;36(3):612–623.
97. Rajaram S, Swift AJ, Capener D, et al. Diagnostic accuracy of contrast-enhanced MR angiography and unenhanced proton MR imaging compared with CT pulmonary angiography in chronic thromboembolic pulmonary hypertension. Eur Radiol 2012;22(2):310–317.
98. Swift AJ, Rajaram S, Condliffe R, et al. Pulmonary artery relative area change detects mild elevations in pulmonary vascular resistance and predicts adverse outcome in pulmonary hypertension. Invest Radiol 2012;47(10):571–577.
99. Gan CT, Lankhaar JW, Westerhof N, et al. Noninvasively assessed pulmonary artery stiffness predicts mortality in pulmonary arterial hypertension. Chest 2007;132(6):1906–1912.
100. Swift AJ, Capener D, Johns C, et al. Magnetic Resonance Imaging in the Prognostic Evaluation of Patients with Pulmonary Arterial Hypertension. Am J Respir Crit Care Med 2017;196(2):228–239.
101. Baggen VJ, Leiner T, Post MC, et al. Cardiac magnetic resonance findings predicting mortality in patients with pulmonary arterial hypertension: a systematic review and meta-analysis. Eur Radiol 2016;26(11):3771–3780.
102. Ohno Y, Higashino T, Takenaka D, et al. MR angiography with sensitivity encoding (SENSE) for suspected pulmonary embolism: comparison with MDCT and ventilation-perfusion scintigraphy. AJR Am J Roentgenol 2004;183(1):91–98.
103. Kluge A, Luboldt W, Bachmann G. Acute pulmonary embolism to the subsegmental level: diagnostic accuracy of three MRI techniques compared with 16-MDCT. AJR Am J Roentgenol 2006;187(1):W7–W14.
104. Repplinger MD, Nagle SK, Harringa JB, et al. Clinical outcomes after magnetic resonance angiography (MRA) versus computed tomographic angiography (CTA) for pulmonary embolism evaluation. Emerg Radiol 2018;25(5):469–477.
105. Sostman HD, Jablonski KA, Woodard PK, et al. Factors in the technical quality of gadolinium enhanced magnetic resonance angiography for pulmonary embolism in PIOPED III. Int J Cardiovasc Imaging 2012;28(2):303–312.

106. Brau AC, Beatty PJ, Skare S, Bammer R. Comparison of reconstruction accuracy and efficiency among autocalibrating data-driven parallel imaging methods. Magn Reson Med 2008;59(2):382–395.
107. Rajaram S, Swift AJ, Capener D, et al. Lung morphology assessment with balanced steady-state free precession MR imaging compared with CT. Radiology 2012;263(2):569–577.
108. Dournes G, Grodzki D, Macey J, et al. Quiet Submillimeter MR Imaging of the Lung Is Feasible with a PETRA Sequence at 1.5 T. Radiology 2015;276(1):258–265.
109. Ohno Y, Koyama H, Yoshikawa T, et al. Pulmonary high-resolution ultrashort TE MR imaging: Comparison with thin-section standard- and low-dose computed tomography for the assessment of pulmonary parenchyma diseases. J Magn Reson Imaging 2016;43(2):512–532.
110. Wielpütz MO, Lee HY, Koyama H, et al. Morphologic Characterization of Pulmonary Nodules With Ultrashort TE MRI at 3T. AJR Am J Roentgenol 2018;210(6):1216–1225.
111. Ohno Y, Koyama H, Yoshikawa T, et al. T2* measurements of 3-T MRI with ultrashort TEs: capabilities of pulmonary function assessment and clinical stage classification in smokers. AJR Am J Roentgenol 2011;197(2):W279–W285.
112. Sørensen L, Nielsen M, Petersen J, Pedersen JH, Dirksen A, de Bruijne M. Chronic Obstructive Pulmonary Disease Quantification Using CT Texture Analysis and Densitometry: Results From the Danish Lung Cancer Screening Trial. AJR Am J Roentgenol 2020;214(6):1269–1279.
113. van Beek EJ, Dahmen AM, Stavngaard T, et al. Hyperpolarised 3He MRI versus HRCT in COPD and normal volunteers: PHIL trial. Eur Respir J 2009;34(6):1311–1321.
114. Salerno M, de Lange EE, Altes TA, Truwit JD, Brookeman JR, Mugler JP 3rd. Emphysema: hyperpolarized helium 3 diffusion MR imaging of the lungs compared with spirometric indexes--initial experience. Radiology 2002;222(1):252–260.
115. Salerno M, Altes TA, Brookeman JR, de Lange EE, Mugler JP 3rd. Rapid hyperpolarized 3He diffusion MRI of healthy and emphysematous human lungs using an optimized interleaved-spiral pulse sequence. J Magn Reson Imaging 2003;17(5):581–588.
116. Wang C, Mugler JP 3rd, de Lange EE, Patrie JT, Mata JF, Altes TA. Lung injury induced by secondhand smoke exposure detected with hyperpolarized helium-3 diffusion MR. J Magn Reson Imaging 2014;39(1):77–84.
117. Kirby M, Mathew L, Wheatley A, Santyr GE, McCormack DG, Parraga G. Chronic obstructive pulmonary disease: longitudinal hyperpolarized (3)He MR imaging. Radiology 2010;256(1):280–289.
118. Kirby M, Mathew L, Heydarian M, Etemad-Rezai R, McCormack DG, Parraga G. Chronic obstructive pulmonary disease: quantification of bronchodilator effects by using hyperpolarized ^{3}He MR imaging. Radiology 2011;261(1):283–292.
119. Kirby M, Pike D, Coxson HO, McCormack DG, Parraga G. Hyperpolarized (3)He ventilation defects used to predict pulmonary exacerbations in mild to moderate chronic obstructive pulmonary disease. Radiology 2014;273(3):887–896.
120. Marshall H, Deppe MH, Parra-Robles J, et al. Direct visualisation of collateral ventilation in COPD with hyperpolarised gas MRI. Thorax 2012;67(7):613–617.
121. Swift AJ, Wild JM, Fichele S, et al. Emphysematous changes and normal variation in smokers and COPD patients using diffusion 3He MRI. Eur J Radiol 2005;54(3):352–358.
122. Fain SB, Panth SR, Evans MD, et al. Early emphysematous changes in asymptomatic smokers: detection with 3He MR imaging. Radiology 2006;239(3):875–883.
123. Chan HF, Stewart NJ, Norquay G, Collier GJ, Wild JM. 3D diffusion-weighted ^{129} Xe MRI for whole lung morphometry. Magn Reson Med 2018;79(6):2986–2995.
124. Jang YM, Oh YM, Seo JB, et al. Quantitatively assessed dynamic contrast-enhanced magnetic resonance imaging in patients with chronic obstructive pulmonary disease: correlation of perfusion parameters with pulmonary function test and quantitative computed tomography. Invest Radiol 2008;43(6):403–410.
125. Hueper K, Parikh MA, Prince MR, et al. Quantitative and semiquantitative measures of regional pulmonary microvascular perfusion by magnetic resonance imaging and their relationships to global lung perfusion and lung diffusing capacity: the multiethnic study of atherosclerosis chronic obstructive pulmonary disease study. Invest Radiol 2013;48(4):223–230.
126. Hueper K, Vogel-Claussen J, Parikh MA, et al. Pulmonary Microvascular Blood Flow in Mild Chronic Obstructive Pulmonary Disease and Emphysema. The MESA COPD Study. Am J Respir Crit Care Med 2015;192(5):570–580.
127. Thomashow MA, Shimbo D, Parikh MA, et al. Endothelial microparticles in mild chronic obstructive pulmonary disease and emphysema. The Multi-Ethnic Study of Atherosclerosis Chronic Obstructive Pulmonary Disease study. Am J Respir Crit Care Med 2013;188(1):60–68.
128. Doyle MF, Tracy RP, Parikh MA, et al. Endothelial progenitor cells in chronic obstructive pulmonary disease and emphysema. PLoS One 2017;12(3):e0173446.
129. Fan L, Xia Y, Guan Y, et al. Capability of differentiating smokers with normal pulmonary function from COPD patients: a comparison of CT pulmonary volume analysis and MR perfusion imaging. Eur Radiol 2013;23(5):1234–1241.
130. Fan L, Xia Y, Guan Y, Zhang TF, Liu SY. Characteristic features of pulmonary function test, CT volume analysis and MR perfusion imaging in COPD patients with different HRCT phenotypes. Clin Respir J 2014;8(1):45–54.
131. Sergiacomi G, Taglieri A, Chiaravalloti A, et al. Acute COPD exacerbation: 3 T MRI evaluation of pulmonary regional perfusion--preliminary experience. Respir Med 2014;108(6):875–882.
132. Ohno Y, Iwasawa T, Seo JB, et al. Oxygen-enhanced magnetic resonance imaging versus computed tomography: multicenter study for clinical stage classification of smoking-related chronic obstructive pulmonary disease. Am J Respir Crit Care Med 2008;177(10):1095–1102.
133. Ma W, Sheikh K, Svenningsen S, et al. Ultra-short echo-time pulmonary MRI: evaluation and reproducibility in COPD subjects with and without bronchiectasis. J Magn Reson Imaging 2015;41(5):1465–1474.
134. Gutberlet M, Kaireit TF, Voskrebenzev A, et al. Free-breathing Dynamic ^{19}F Gas MR Imaging for Mapping of Regional Lung Ventilation in Patients with COPD. Radiology 2018;286(3):1040–1051.
135. Halaweish AF, Moon RE, Foster WM, et al. Perfluoropropane gas as a magnetic resonance lung imaging contrast agent in humans. Chest 2013;144(4):1300–1310.
136. Voskrebenzev A, Gutberlet M, Klimeš F, et al. Feasibility of quantitative regional ventilation and perfusion mapping with phase-resolved functional lung (PREFUL) MRI in healthy volunteers and COPD, CTEPH, and CF patients. Magn Reson Med 2018;79(4):2306–2314.
137. Kirby M, Pike D, McCormack DG, Lam S, Coxson HO, Parraga G. Longitudinal Computed Tomography and Magnetic Resonance Imaging of COPD: Thoracic Imaging Network of Canada (TINCan) Study Objectives. Chronic Obstr Pulm Dis (Miami) 2014;1(2):200–211.
138. Chan HF, Collier GJ, Weatherley ND, Wild JM. Comparison of in vivo lung morphometry models from 3D multiple b-value ^{3} He and ^{129} Xe diffusion-weighted MRI. Magn Reson Med 2019;81(5):2959–2971.
139. Stewart NJ, Chan HF, Hughes PJC, et al. Comparison of ^{3} He and ^{129} Xe MRI for evaluation of lung microstructure and ventilation at 1.5T. J Magn Reson Imaging 2018;48(3):632–642.
140. Kirby M, Svenningsen S, Owrangi A, et al. Hyperpolarized 3He and 129Xe MR imaging in healthy volunteers and patients with chronic obstructive pulmonary disease. Radiology 2012;265(2):600–610.
141. Woolcock AJ. Epidemiology of chronic airways disease. Chest 1989;96(3,Suppl):302S–306S.
142. To T, Stanojevic S, Moores G, et al. Global asthma prevalence in adults: findings from the cross-sectional world health survey. BMC Public Health 2012;12(1):204.
143. Bhatt SP, Soler X, Wang X, et al. Association between Functional Small Airway Disease and FEV1 Decline in Chronic Obstructive Pulmonary Disease. Am J Respir Crit Care Med 2016;194(2):178–184.
144. Aysola RS, Hoffman EA, Gierada D, et al. Airway remodeling measured by multidetector CT is increased in severe asthma and correlates with pathology. Chest 2008;134(6):1183–1191.
145. Capaldi DPI, Sheikh K, Eddy RL, et al. Free-breathing Functional Pulmonary MRI: Response to Bronchodilator and Bronchoprovocation in Severe Asthma. Acad Radiol 2017;24(10):1268–1276.
146. Pennati F, Quirk JD, Yablonskiy DA, Castro M, Aliverti A, Woods JC. Assessment of regional lung function with multivolume (1)H MR imaging in health and obstructive lung disease: comparison with (3)He MR imaging. Radiology 2014;273(2):580–590.
147. Altes TA, Powers PL, Knight-Scott J, et al. Hyperpolarized 3He MR lung ventilation imaging in asthmatics: preliminary findings. J Magn Reson Imaging 2001;13(3):378–384.
148. Samee S, Altes T, Powers P, et al. Imaging the lungs in asthmatic patients by using hyperpolarized helium-3 magnetic resonance: assessment of response to methacholine and exercise challenge. J Allergy Clin Immunol 2003;111(6):1205–1211.
149. Svenningsen S, Kirby M, Starr D, et al. Hyperpolarized (3) He and (129) Xe MRI: differences in asthma before bronchodilation. J Magn Reson Imaging 2013;38(6):1521–1530.
150. Ebner L, He M, Virgincar RS, et al. Hyperpolarized 129Xenon Magnetic Resonance Imaging to Quantify Regional Ventilation Differences in Mild to Moderate Asthma: A Prospective Comparison Between Semiautomated

Ventilation Defect Percentage Calculation and Pulmonary Function Tests. Invest Radiol 2017;52(2):120–127.
151. de Lange EE, Altes TA, Patrie JT, et al. Evaluation of asthma with hyperpolarized helium-3 MRI: correlation with clinical severity and spirometry. Chest 2006;130(4):1055–1062.
152. de Lange EE, Altes TA, Patrie JT, et al. The variability of regional airflow obstruction within the lungs of patients with asthma: assessment with hyperpolarized helium-3 magnetic resonance imaging. J Allergy Clin Immunol 2007;119(5):1072–1078.
153. Aysola R, de Lange EE, Castro M, Altes TA. Demonstration of the heterogeneous distribution of asthma in the lungs using CT and hyperpolarized helium-3 MRI. J Magn Reson Imaging 2010;32(6):1379–1387.
154. Altes TA, Mugler JP 3rd, Ruppert K, et al. Clinical correlates of lung ventilation defects in asthmatic children. J Allergy Clin Immunol 2016;137(3):789–96.e7, e787.
155. Kruger SJ, Niles DJ, Dardzinski B, et al. Hyperpolarized Helium-3 MRI of exercise-induced bronchoconstriction during challenge and therapy. J Magn Reson Imaging 2014;39(5):1230–1237.
156. Horn FC, Marshall H, Collier GJ, et al. Regional Ventilation Changes in the Lung: Treatment Response Mapping by Using Hyperpolarized Gas MR Imaging as a Quantitative Biomarker. Radiology 2017;284(3):854–861.
157. Mummy DG, Carey KJ, Evans MD, et al. Ventilation defects on hyperpolarized helium-3 MRI in asthma are predictive of 2-year exacerbation frequency. J Allergy Clin Immunol 2020. 10.1016/j.jaci.2020.02.029. Published online March 13, 2020.
158. Woodhouse N, Wild JM, Paley MN, et al. Combined helium-3/proton magnetic resonance imaging measurement of ventilated lung volumes in smokers compared to never-smokers. J Magn Reson Imaging 2005;21(4):365–369.
159. Svenningsen S, Nair P, Guo F, McCormack DG, Parraga G. Is ventilation heterogeneity related to asthma control? Eur Respir J 2016;48(2):370–379.
160. Svenningsen S, Eddy RL, Lim HF, Cox PG, Nair P, Parraga G. Sputum Eosinophilia and Magnetic Resonance Imaging Ventilation Heterogeneity in Severe Asthma. Am J Respir Crit Care Med 2018;197(7):876–884.
161. Svenningsen S, Haider E, Boylan C, et al. CT and Functional MRI to Evaluate Airway Mucus in Severe Asthma. Chest 2019;155(6):1178–1189.
162. Ohno Y, Nishio M, Koyama H, et al. Pulmonary MR imaging with ultra-short TEs: utility for disease severity assessment of connective tissue disease patients. Eur J Radiol 2013;82(8):1359–1365.
163. Pinal-Fernandez I, Pineda-Sanchez V, Pallisa-Nuñez E, et al. Fast 1.5 T chest MRI for the assessment of interstitial lung disease extent secondary to systemic sclerosis. Clin Rheumatol 2016;35(9):2339–2345.
164. Stadler A, Jakob PM, Griswold M, Stiebellehner L, Barth M, Bankier AA. T1 mapping of the entire lung parenchyma: Influence of respiratory phase and correlation to lung function test results in patients with diffuse lung disease. Magn Reson Med 2008;59(1):96–101.
165. Buzan MT, Eichinger M, Kreuter M, et al. T2 mapping of CT remodelling patterns in interstitial lung disease. Eur Radiol 2015;25(11):3167–3174.
166. Marinelli JP, Levin DL, Vassallo R, et al. Quantitative assessment of lung stiffness in patients with interstitial lung disease using MR elastography. J Magn Reson Imaging 2017;46(2):365–374.
167. Müller CJ, Schwaiblmair M, Scheidler J, et al. Pulmonary diffusing capacity: assessment with oxygen-enhanced lung MR imaging preliminary findings. Radiology 2002;222(2):499–506.
168. Ohno Y, Nishio M, Koyama H, et al. Oxygen-enhanced MRI for patients with connective tissue diseases: comparison with thin-section CT of capability for pulmonary functional and disease severity assessment. Eur J Radiol 2014;83(2):391–397.
169. Molinari F, Eichinger M, Risse F, et al. Navigator-triggered oxygen-enhanced MRI with simultaneous cardiac and respiratory synchronization for the assessment of interstitial lung disease. J Magn Reson Imaging 2007;26(6):1523–1529.
170. Takenaka D, Puderbach M, Ohno Y, et al. Oxygen-enhanced lung magnetic resonance imaging: influence of inversion pulse slice selectivity on inversion recovery half-Fourier single-shot turbo spin-echo signal. Jpn J Radiol 2011;29(4):244–250.
171. Kaushik SS, Freeman MS, Yoon SW, et al. Measuring diffusion limitation with a perfusion-limited gas--hyperpolarized 129Xe gas-transfer spectroscopy in patients with idiopathic pulmonary fibrosis. J Appl Physiol (1985) 2014;117(6):577–585.
172. Wang JM, Robertson SH, Wang Z, et al. Using hyperpolarized ^{129}Xe MRI to quantify regional gas transfer in idiopathic pulmonary fibrosis. Thorax 2018;73(1):21–28.
173. Weatherley ND, Stewart NJ, Chan HF, et al. Hyperpolarised xenon magnetic resonance spectroscopy for the longitudinal assessment of changes in gas diffusion in IPF. Thorax 2019;74(5):500–502.
174. Rankine LJ, Wang Z, Wang JM, et al. ^{129}Xenon Gas Exchange Magnetic Resonance Imaging as a Potential Prognostic Marker for Progression of Idiopathic Pulmonary Fibrosis. Ann Am Thorac Soc 2020;17(1):121–125.
175. Yi CA, Lee KS, Han J, Chung MP, Chung MJ, Shin KM. 3-T MRI for differentiating inflammation- and fibrosis-predominant lesions of usual and nonspecific interstitial pneumonia: comparison study with pathologic correlation. AJR Am J Roentgenol 2008;190(4):878–885.
176. Biederer J, Ohno Y, Hatabu H, et al. Screening for lung cancer: Does MRI have a role? Eur J Radiol 2017;86:353–360.
177. Allen BD, Schiebler ML, Sommer G, et al. Cost-effectiveness of lung MRI in lung cancer screening. Eur Radiol 2020;30(3):1738–1746.